Aquatic carbon fluxes dampen the overall variation of net ecosystem productivity in the Amazon basin: An analysis of the interannual variability in the boundless carbon cycle

Aquatic carbon fluxes dampen the overall variation of net ecosystem productivity in the Amazon basin: An analysis of the interannual variability in the boundless carbon cycle.

Adam Hastie[1] | Ronny Lauerwald[1,2] | Philippe Ciais[3] | Pierre Regnier[1]

[1]Biogeochemistry and Earth System Modelling, Department of Geoscience, Environment and Society, Universite Libre de Bruxelles, Bruxelles, Belgium

[2]College of Engineering, Mathematics and Physical Sciences, University of Exeter, Exeter, UK

[3]Laboratoire des Sciences du Climat et de l'Environnement, UMR8212, CEA-CNRS-UVSQ F-91191 Gif sur Yvette, France

Abstract

The river-floodplain network plays an important role in the carbon (C) budget of the Amazon basin, as it transports and processes a significant fraction of the C fixed by terrestrial vegetation, most of which evades as CO_2 from rivers and floodplains back to the atmosphere. There is empirical evidence that exceptionally dry or wet years have an impact on the net C balance in the Amazon. While seasonal and interannual variations in hydrology have a direct impact on the amounts of C transferred through the river-floodplain system, it is not known how far the variation of these fluxes affects the overall Amazon C budget.

Here, we introduce a new wetland forcing file for the ORCHILEAK model, which improves the representation of floodplain dynamics and allows us to closely reproduce data-driven estimates of net C exports through the river-floodplain network. Based on this new wetland forcing and two climate forcing datasets, we show that across the Amazon, the percentage of NPP lost to the river-floodplain system is highly variable at the interannual timescale and wet years fuel aquatic CO_2 evasion. However, at the same time overall net ecosystem productivity (NEP) and C sequestration is highest during wet years, partly due to reduced decomposition rates in water-logged floodplain soils. It is years with the lowest discharge and floodplain inundation, often associated with El Nino events, that have the lowest NEP and the highest total (terrestrial plus aquatic) CO_2 emissions back to atmosphere. Furthermore, we find that aquatic C fluxes display greater variation than terrestrial C fluxes, and that this variation significantly dampens the interannual variability in NEP of the Amazon basin. These results

call for a more integrative view of the C fluxes through the vegetation-soil-river-floodplain continuum, which directly places aquatic C fluxes into the overall C budget of the Amazon basin.

1. Introduction

The land-ocean aquatic continuum (LOAC) is now well established as an important component of the global carbon (C) cycle (Ciais et al., 2013). Atmospheric C fixed in terrestrial ecosystems and wetlands can be lost through respiration, and stored in biomass and soil, but can also be transferred laterally to the LOAC as dissolved organic carbon (DOC), particulate organic carbon (POC) and dissolved CO_2. Along the LOAC this C can in turn undergo biogeochemical transformations, be lost back to the atmosphere via CO_2 evasion, transferred further downstream to estuaries and the coast, or undergo sedimentation in wetlands (incl. lakes and reservoirs). It has been demonstrated at the catchment (Cole & Caraco, 2001) to global scale (Battin et al., 2009; Regnier et al., 2013; Ciais et al. in review), that these fluxes are important and should not be neglected in land C budgets.

Globally, there remains a high degree of uncertainty associated with the amounts of C being transferred through and processed within the LOAC. Estimates of the total amount of terrestrial C inputs to inland waters range widely from 1.1 to 5.1 Pg C yr^{-1} (Cole at al., 2007; Aufdenkampe et al., 2011; Regnier et al., 2013; Drake et al., 2017), reflecting the fact that this flux is indirectly derived by summing estimates of aquatic CO_2 evasion, C exports to the coast and burial in the LOAC. Of the three constituent fluxes, CO_2 evasion is the largest (Drake et al., 2017) and thus uncertainties in CO_2 evasion dominate the subsequent uncertainty in the export of terrestrial C to inland waters. Moreover, aquatic CO_2 evasion is highly spatially variable and hotspot regions have been identified; the boreal and tropical

56 regions contributing disproportionately to global CO_2 evasion from lakes (Hastie et al., 2018)
57 and rivers (Lauerwald et al., 2015), respectively.

58 In the Tropics, high terrestrial net primary productivity (NPP) and high rainfall drive a large
59 export of C to inland waters and in turn high aquatic CO_2 evasion. In 2002, Richey et al.
60 extrapolated observed pCO_2 measurements to estimate a total CO_2 evasion flux of 0.47 Pg C
61 yr^{-1} from the inland waters of the Amazon Basin (upstream of Obidos, see Fig. S1), 13 times
62 greater than their 36 Tg C yr^{-1} estimate of the total organic C (TOC) export to the coast. In
63 2013, Rasera et al. calculated a substantially higher CO_2 evasion of 0.8 Pg C yr^{-1} over the
64 same basin area, largely as a result of higher values of gas exchange velocity (K_{600}). More
65 recently, Sawakuchi et al. (2017) added observations from the basin area downstream of
66 Obidos and concluded that CO_2 evasion from the entire Amazon Basin (down to mouth)
67 could potentially be as high as 1.39 Pg C yr^{-1}.

68 Previous studies have shown that there is considerable seasonal variation in aquatic CO_2
69 evasion. Richey et al. (2002), found that the partial pressure of CO_2 (pCO_2) and in turn CO_2
70 evasion was tightly coupled to discharge, increasing and decreasing with rising and falling
71 water respectively. Moreover, they measured exceptionally high pCO_2 values (>44,000 µatm)
72 on the floodplain of the mainstem of the Amazon, and speculated that the source of the C is
73 likely to be organic matter exported from flooded forests.

74 This was later confirmed by Abril et al. (2014) who demonstrated that Amazonian wetlands
75 export around 50% of their GPP to inland waters in contrast to the typical values of <2%
76 exported from terrestrial landscapes. They went on to conclude that the lateral C flux from
77 wetlands is enough to account for around 210 Tg C yr^{-1} of the total CO_2 evasion flux from the
78 inland waters of the Amazon river-floodplain network. A recent study by Almeida et al
79 (2017) demonstrated that in addition to seasonal variation, large flood events also drive

interannual variation in CO_2 evasion from the Madeira River (a tributary of the Amazon), namely that years with extreme flooding evade 20% more CO_2 to the atmosphere per unit area than years without. Another flux linked to flood events is C burial and a recent study estimated the POC burial flux in Amazon floodplain lakes at 16 Tg C yr^{-1} (Sanders et al., 2017), at least an order of magnitude lower than estimates of CO_2 evasion.

These observed seasonal and interannual signals in C fluxes are particularly important given that the region is increasingly vulnerable to extreme climatic events such as droughts and floods (Marengo et al., 2011; Chou et al., 2013; Gloor et al., 2013; Zulkafli et al., 2016). Indeed, recent studies have shown substantial decreases in terrestrial net primary productivity (NPP), and in turn C uptake from the atmosphere as a result of the 2005 and 2010 droughts (Zhao & Running, 2010; Potter et al, 2011; Gatti et al., 2014; Doughty et al., 2015 and Feldpausch et al., 2016). However, most of these studies do not account for LOAC fluxes. For these reasons, it is important that we understand the interannual variation in LOAC fluxes and how they influence the overall net ecosystem production (NEP) of the entire Amazon Basin.

With this in mind, we aim to tackle the following research questions:

- To what extent do the LOAC fluxes (aquatic CO_2 evasion and C export to the coast) vary inter-annually and seasonally throughout the entire Amazon Basin?
- How does interannual variation in discharge and flooding affect the LOAC fluxes, terrestrial NPP, soil heterotrophic respiration (SHR) and ultimately the NEP of the Amazon Basin, particularly in the context of increasing climatic extremes? More specifically, does the incorporation of LOAC fluxes amplify or dampen variation in NEP?

103 Upscaling studies and empirical models are useful in providing estimates of individual
104 components of the LOAC fluxes for the present day. However, these methods cannot
105 represent the interaction between the different aspects of the Amazon Basin C cycle. A more
106 complex and integrated modelling approach is required to understand and, ultimately, predict
107 the longer-term variation in LOAC fluxes and how this variation affects the net C balance of
108 these ecosystems.

109 In 2017, Lauerwald et al. developed the first full Land Surface Model (ORCHILEAK model)
110 approach to represent the lateral C fluxes along the LOAC in the Amazon Basin and similarly
111 demonstrated the significance of wetlands, concluding that 51% of total CO_2 evasion comes
112 from the floodplains. The study estimated a total CO_2 evasion of 379 C Tg yr^{-1}, close to the
113 value produced by Richey et al. from up-scaling of measurements. In addition, they
114 substantiated the idea that wetlands are a disproportionately important source of C to rivers,
115 calculating that the CO_2 inputs from root and heterotrophic respiration in flooded soils are
116 almost twice that from non-flooded soils.

117 The land surface model approach undertaken by Lauerwald et al. (2017) provides a valuable
118 tool for further research, in particular the capability to make future projections of the LOAC
119 C fluxes. However, while they were able to reproduce the seasonality in discharge on the
120 main stem of the Amazon, the total flooded area was substantially underestimated when
121 compared to the observed data of Richey et al., 2013 (after Hess et al., 2003). This is because
122 Lauerwald et al. (2017) relied on the coarse (0.25°) global inundation dataset of Prigent et al.
123 (2007), which tends to underestimate the total floodable area (Lauerwald et al., 2017). Given
124 previous estimates of the magnitude of the CO_2 evasion flux from the Amazon floodplain, the
125 importance of wetlands, and the region's increasing vulnerability to climatic extremes; it is
126 vital that we can accurately model its floodplain dynamics.

In this study, an improved representation of floodplain and wetland dynamics is achieved through the production of a new floodplain forcing file for the ORCHILEAK model, from the high resolution (100m or 0.0008°) synthetic aperture radar (SAR) dataset of Hess et al. (2015). We use this new forcing file to improve the simulation of the interannual variation of LOAC fluxes. In turn, we are able to address the research questions previously outlined, and more specifically to evaluate the impact of flood extent on the dynamics of LOAC fluxes, and ultimately how interannual variation in these aquatic C fluxes influences the overall variation in NEP in the Amazon.

2. Methods

2.1 A brief description of the ORCHILEAK land surface model

ORCHILEAK (Lauerwald et al., 2017) is a new model branch of ORCHIDEE (Organizing Carbon and Hydrology in Dynamic Ecosystems) (Krinner et al. 2005), the land surface component of the Institut Pierre-Simon Laplace (IPSL) earth system model (ESM). It simulates the production of DOC in the canopy and soils, the leaching of DOC and CO_2 from soils to the river network, DOC mineralization and the subsequent CO_2 evasion from the water surface. Crucially, it also simulates the exchange of C between litter, soils and water on floodplains and in swamps. The representation of these fluxes is in turn closely coupled to the hydrology scheme, namely the representation of precipitation, throughfall, surface runoff, drainage, and the routing of discharge along the river-floodplain network. At the same time, ORCHILEAK also simulates vegetation dynamics of 12 plant functional types, 5 of which are present in the Amazon, as well as the C balance of biomass, litter and soils. In short, ORCHILEAK integrates LOAC fluxes within a full representation of the terrestrial C cycling as simulated by ORCHIDEE. However, in its current form ORCHILEAK does not account

for the burial of POC in fluvial and floodplain sediments or the evasion of C to the atmosphere as CH_4. These fluxes are further discussed later. While the model does not simulate the lateral transport of POC, it does account for the decomposition of submerged litter as a substantial source of DOC and dissolved CO_2 to the water column; in other words, POC from submerged litter is assumed to decompose locally in ORCHILEAK. The model is described in more detail in the proceeding sections. For a full model description, as well as a discussion on model assumptions and limitations, please refer to Lauerwald et al. (2017).

2.2 Overview of the hydrology, soil C scheme, and the transport and transformation of aquatic C fluxes in ORCHILEAK

Precipitation and other meteorological input parameters are prescribed by a forcing file. The hydrology module of ORCHILEAK, just like that of the standard version of ORCHIDEE, partitions the precipitation between interception loss in the vegetation canopy and throughfall to the ground. The throughfall is further partitioned into infiltration and surface runoff. The soil water storage is refilled by infiltration and depleted by evapotranspiration and drainage. The soil hydrology is represented using a 2 m soil column vertically discretized into 11 layers of geometrically increasing thickness from top to bottom. These processes are all represented at a 30 min time step (see d'Orgeval et al., 2008, Rosnay et al., 2002 for details).

ORCHILEAK incorporates a soil C module largely based on ORCHIDEE-SOM (Camino-Serrano, 2018). The soil module uses the hydrological module outputs to simulate microbial production and consumption of DOC, sorption and desorption of DOC on soil organic matter, the advection and diffusion of DOC and dissolved CO_2 within the soil column and their subsequent lateral export via runoff and drainage as well as the throughfall of DOC onto the soil or water surface. There are 3 pools of DOC in the soil which are defined by their source material and residence times (τ_{carbon}); the active, slow and passive pool. ORCHILEAK

distinguishes between flooded and non-flooded soils; decomposition rates of litter, SOC and DOC being 3 times lower in flooded soils. Furthermore, it simulates the input of C to the water column from flooded soils; DOC from litter and SOC decomposition from the top 4.5 cm of the soil column feeds directly to the DOC pool of the overlying waterbody.

The river routing module of ORCHILEAK routes the runoff and drainage from the hydrology module and the corresponding dissolved C fluxes from the soil C module as river flow at a daily time-step along a gridded river routing scheme at 0.5° resolution (Vorosmarty et al., 2000). The river network is connected to two sorts of wetland, floodplains and swamps. Where a swamp is present, a constant fraction of the river flow is feeding into the bottom of the soil column. Where a floodplain is present, a temporary water body of time-variant surface and volume may be formed beside the river channel and it is fed by a fraction of river flow when bank-full discharge is surpassed. In the case of the Amazon basin, the bankfull discharge threshold was defined as the median discharge simulated over the period 1980-2000 (see Lauerwald et al., 2017). From the inundated floodplain, water and dissolved C may infiltrate back into the soil or flow back into the river channel, while water may also evaporate. The maximal floodable area (MFF) and the areal fraction of swamps (MFS) per simulation grid is prescribed by a forcing file. The water that infiltrates back into the soil is returned to the hydrology module. The dissolved C contained in that water is returned to the soil C module.

ORCHILEAK simulates the transport and decomposition of terrestrial C inputs within the routing scheme, with the assumption that the lateral transport of DOC and CO_2 are proportional to discharge. Within the water column, DOC is separated into a labile and refractory pool, with half-life times of 2 and 80 days, respectively. The labile pool corresponds to the active pool of the soil C scheme, while the refractory pool is derived from the slow and passive soil solution DOC pools combined. In order to ensure numerical

precision, CO_2 production and evasion from the water column, as well CO_2 inputs from flooded litter and SOC are simulated at the high temporal resolution of 1/240 day (6 min). pCO_2 is calculated at the same 6 min time-step based on the dissolved CO_2 concentration, and the temperature-dependent solubility of CO_2. pCO_2 is then used along with a gas exchange velocity and a diurnally variable water surface area, to calculate CO_2 evasion. Fixed gas exchange values of 3.5 m d^{-1} and 0.65 m d^{-1} are used for rivers (and open floodplains) and forested floodplains, respectively. Flooded forests are given a lower gas exchange velocity due to the reduced impact of wind (i.e. lower wind speeds). For a more detailed explanation, see Lauerwald et al. (2017).

2.3 New wetland forcing files

The original routing scheme of ORCHIDEE used universal MFF and MFS derived from the Global Lakes and Wetlands Database (GLWD, Lehner and Doll, 2004) that were shown to considerably underestimate inundated areas in the Amazon (Guimberteau et al., 2012). As a result, Guimberteau et al. developed new MFF and MFS based on the 0.25° datasets of Prigent et al. (2007) and Martinez and Le Toan (2007), respectively. This led to some improvement but inundation was still substantially underestimated in the Amazon Basin.

In the Guimberteau datasets, “swamps”, defined as the vegetated part of maximum floodplain, were subtracted from the MFF and used to create the separate swamp (MFS) forcing file. In ORCHILEAK (Lauerwald et al., 2017), swamps were reincorporated into the MFF forcing file, creating a larger, more realistic MFF, and representing the total flooded area from which inland water CO_2 is evading. While these modifications again led to some improvement in the representation of floodplains and swamps in ORCHILEAK, it fundamentally still relied on a low resolution (0.25°) dataset, missing smaller areas of

223 inundation, and meaning that the overall maximum floodplain extent was too small
224 (Lauerwald et al., 2017).

225 With these limitations in mind, we created a new maximal fraction of floodplain (MFF,
226 Fig.1) forcing file for the ORCHILEAK model based on the 100m Synthetic Aperture Radar
227 (SAR) data described in Hess et al. (2015, see Fig.1 a). This dataset represents different
228 wetland types during the 1996 May-June flood season. Firstly, we merged all of the wetland
229 categories in Fig. 1 a) into one class, with the exception of the 'non-wetland within the
230 Amazon Basin', 'Open water' and 'Elevation >= 500 m, in Basin' categories. We then
231 aggregated the merged dataset to a resolution of 0.5° (Fig.1 b). Note that in the MFF we
232 included three classes of land cover that were not flooded during the 1996 flood season,
233 namely 'non-flooded shrubs', 'non-flooded woodlands' and 'non-flooded forest' (classes 44,
234 66 and 88). This decision is based on the justification provided in Hess et al. that these "areas
235 not flooded on either date, but adjacent to flooded areas and displaying landforms consistent
236 with wetland geomorphology". In other words, while these areas were not flooded in 1996,
237 they are likely prone to inundation in other years with greater precipitation and thus should be
238 included in maximum flood extent. Across the Amazon basin, the new forcing file prescribes
239 an average MFF of 13.6%, approximately twofold greater than the 6.3% produced with the
240 original ORCHILEAK forcing derived from Prigent et al. (2007) (Fig. 1 c, d). The addition
241 of the 44, 66 and 88 land cover classes makes a moderate difference; we produce an average
242 MFF of 10% without these 3 classes. For comparison, we also aggregated the 232m
243 resolution wetland dataset of Gumbricht et al. (2017). Assuming that all of the wetland
244 categories in Gumbricht et al. (2017) contribute to the maximum flood extent, we produce an
245 average MFF of 14.9%. However, we chose to use the MFF derived from Hess et al. (2015)
246 as it is measured at a higher resolution and considers wetlands as synonymous with
247 floodplains, while Gumbricht et al. (2017) has a wider definition. In order to account for the

uncertainty associated with the MFF forcing file we created two new versions of it; one in which the MFF of each grid was systematically increased by 7% (excluding "highland" areas >=500m identified in Hess et al., 2015) (MFF+7), and another where the MFF was decreased by 7% (MFF-7). We chose a value of 7% as this is the inferred error of the original dataset, described in Hess et al. (2015). Across the Amazon basin, the MFF-7 forcing gives an average MFF of 9.3% while the MFF+7 gives an average of 18.3%. This range also envelops the uncertainty associated with the inclusion or exclusion of classes 44, 66 and 88, as well as that associated with the difference between the Hess and Gumbricht datasets.

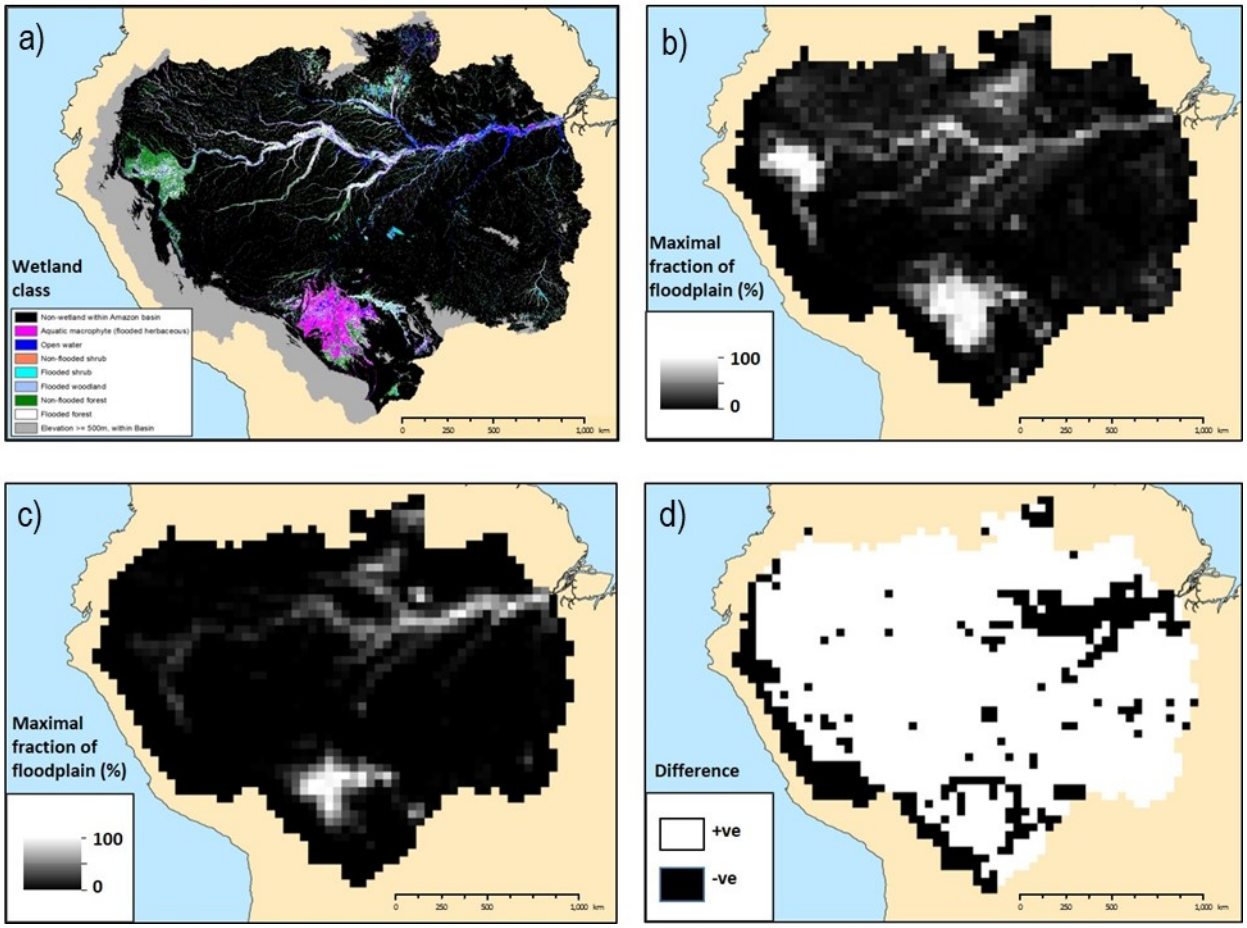

Figure 1. a) Wetland classification within the Amazon Basin (Hess et al., 2015), b); the new maximal fraction of floodplain (MFF) forcing file derived from Hess et al. (2015) data, c) the previous MFF forcing file (Guimberteau et al., 2012) and d) the difference between the new and old MFF. In pane d), "+ve" refers to an increase in MFF with the new MF forcing, while "-ve" refers to a decrease. Maps in panels b-d are at a resolution of 0.5°.

263 We also created a new ORCHILEAK maximal fraction of swamps (MFS, Fig. 2) forcing file
264 based on the 232 m resolution tropical wetland dataset of Gumbricht et al (2017), as the Hess
265 et al. (2015) dataset does not define an explicit "swamp" category. We extracted class 30
266 (Swamps incl. bogs) and 40 (Fens), before merging these classes and aggregating them to the
267 0.5° resolution. Across the Amazon basin, the new forcing file prescribes an average MFS of
268 5.4% (Fig.2, b) which is comparable to the 6% produced with the previous approach
269 (Guimberteau et al., 2012) (Fig. 2, c, d).

270

271

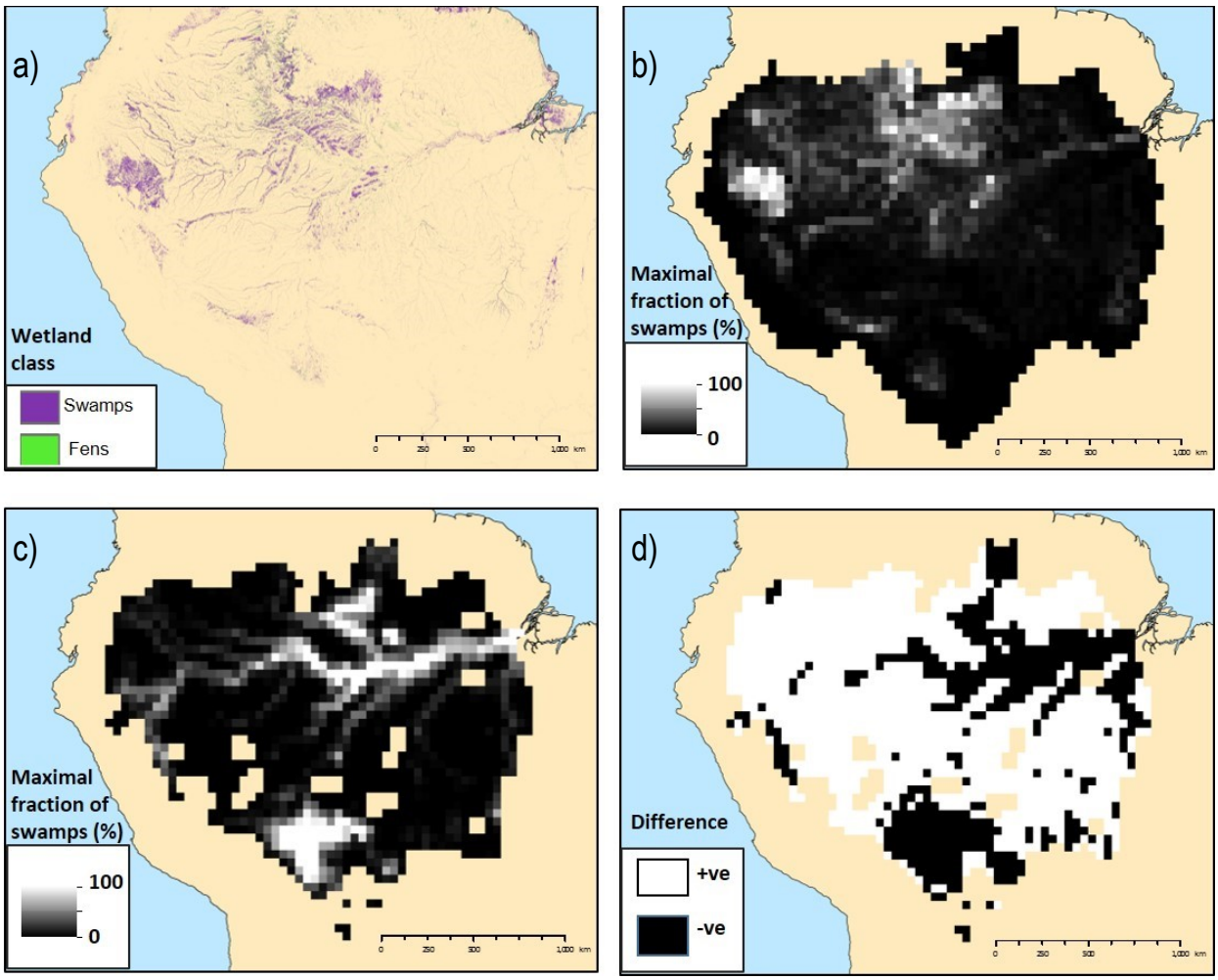

272

273 Figure 2. a) Swamps and ferns classification within Amazon Basin from Gumbricht et al
274 (2017)) b); the new maximal fraction of swamps (MFS) forcing file derived from Gumbricht
275 et al. (2017) data, c); the previous MFS forcing file (Lauerwald et al., 2017) and d) the

difference between the new and old MFS. In pane d), "+ve" refers to an increase in MFF with the new MF forcing, while "-ve" refers to a decrease. Maps in panels b-d are at a resolution of 0.5°.

2.4 Simulation Set-up

Model configuration

The model was initially run from 1980 until 2000 using two different climate forcing datasets, namely Princeton GPCC (Sheffield et al., 2006), and a regionally updated version of NCC (Ngo-Duc et al., 2005) which was introduced by Guimberteau et al. (2012). This was done in order to test which dataset is able to better recreate observed discharge and the associated seasonal and interannual variability in floodplain inundation, as well as to account for the uncertainty associated with choice of climate forcing. With the combination of the two climate forcing files and the three MFF forcing files, we ran six different model configurations. Model parameterisation can also cause uncertainty such as the setting of decomposition rate constants for labile and refractory DOC within ORCHILEAK. However, the impact of these parameters was already investigated via a sensitivity analyses in the paper describing the development of the ORCHILEAK model (Lauerwald et al., 2017). As such, we chose to focus on climate forcing and floodplain area as sources of uncertainty in combination with substantial validation against observations and model outputs from the literature.

The original ORCHILEAK simulation (Lauerwald et al., 2017) used only the updated NCC climate forcing. Here, we ran four simulations with the NCC climate forcing dataset; one with the new versions of MFF (hereafter referred to as "standard MFF") and MFS, two more to account for the uncertainty in MFF (MFF+7 & MFF-7), and another with the old MFF (Lauerwald et al., 2017), in order to determine the impact of the new wetland forcing files.

We ran the Princeton GPCC simulations with the new versions of MFF and MFS only (three runs). Model parameterisation follows Lauerwald et al. (2017).

Hydrology statistics

Following Lauerwald et al. (2017), we calculated a series of statistical parameters in order to calibrate the flood dynamics of the model in a robust and consistent manner. After an initial run, we calculated bank-full discharge and the median water storage for each grid cell (1980-2000), for each model configuration. Any discharge in excess of the median water storage will overtop and begin to inundate the floodplains. After updating bank-full discharge and re-running each model configuration, we calculated the 95th percentile of all simulated water level heights (1980-2000) for each grid cell. This represents the maximum water level, at which the maximum floodable area is inundated. Once this was updated, each model configuration was re-run once more.

Soil carbon spin up

In order to reach a steady state soil carbon pool, we spun-up the model for a total of approximately 7,000 years, looping over 10 years of climate forcing data (1948-1957). To reach steady state more quickly, we first ran the model for 2000 years with the default soil carbon residence time (τ_{carbon}) values halved and a constant atmospheric CO_2 concentration of 350 μatm. Land-cover, representative of the first year of climate forcing data (1948), remained constant over these spin-up runs. After this procedure, all of the soil C pools were approximately at steady state (<0.01% change over the last century of the spin up). Note that it is assumed that soil C pools were in quasi steady state before significant human impact.

Transient simulations

We then performed a transient (industrial) run from 1860, until the year that the particular climate forcing dataset starts from (for example to 1948 for Princeton GPCC), again looping

over 10 years of climate data but with transient land-cover (LUH-CMIP5) and atmospheric CO_2. Finally, we performed a fully transient simulation (land-cover, atmospheric CO_2 and climate) to the final year of each climate forcing dataset. Note that the NCC climate forcing data is only available until 2000 while the Princeton GPCC data runs until 2010.

2.5 Model evaluation and analysis of simulation results

We started by evaluating the hydrology, concentrating on flooded area as this was underestimated in the original ORCHILEAK model set up (Lauerwald et al., 2017). The new MFF and MFS forcing files meant that we had to re-evaluate both discharge and floodplain inundation dynamics. We firstly focused on recreating observed discharge at Obidos (Fig. S1), the most downstream gauging station for which an observed time-series is available (Cochonneau et al., 2006). Total flooded area of the central quadrant of the Amazon basin (Fig. S1) was tested against remote sensing data (Melack et al., 2011). Note that the Melack et al. dataset uses the same wetland mask as we use here, but the seasonality and area of inundation is completely independent. We then performed a model validation for the DOC and aquatic CO_2 evasion fluxes using the same validation data and methodology as described in Lauerwald et al. (2017), as well as an in-depth comparison of our results to those of previous studies. In addition, we examined the interannual variation of both the terrestrial (meaning NPP and SHR) and aquatic C fluxes (also referred to as LOAC fluxes, and meaning CO_2 evasion from the water surface and the export flux of C to the coast) of the Amazon, and assessed how this variation relates to rainfall and temperature variation through linear regression analysis. As we found long-term (decadal) trends in several of the fluxes, most notably NPP (Tables S2 & S3), we detrended the annual times series using the Detrend function within the "SpecsVerification" package in R (R Core Team 2013), before performing the regression analyses using STATISTICA^{TM}. Finally, we sum the various C

fluxes to calculate the net C balance of the Amazon Basin (see 2.6) and examine the importance of the LOAC fluxes to the overall C balance.

2.6 Calculating the net carbon balance of the Amazon

In order to estimate the net C balance of the Amazon basin, we summed the terrestrial and aquatic C fluxes to estimate Net Ecosystem Production (NEP) and Net Biome Production (NBP). Positive values of NEP and NBP correspond to a net sink.

We define NEP as follows:

$$NEP = NPP + TF - SHR - FCO_2 - LE_{\text{Aquatic}} \quad (1)$$

Where *NPP* is terrestrial net primary production, *TF* is the throughfall flux of DOC, *SHR* is soil heterotrophic respiration (only the part evading from the soil surface); FCO_2 is CO_2 evasion from the water surface and $LE_{Aquatic}$ is the export flux of C to the coast. *NBP* is the same as *NEP* but with the addition of the C lost (or gained) through land use change (*LUC*, including fires and the export of woody biomass) and crop harvest (*Harvest*):

$$NBP = NEP - (LUC + Harvest) \quad (2)$$

3. Results

3.1 Representation of Hydrology

The model is able to reproduce river discharge at Obidos (1980-2000), the farthest downstream river gauge (Fig. S1), both in terms of total magnitude and seasonal variability. Simulation with the old floodplain/swamp forcing used by Lauerwald et al. (2017) and simulations based on the new floodplain/swamp forcing file showed a similarly good performance (Fig.3-1a-c, Table 1). There was no substantial difference in the simulated

discharge from the Amazon basin after the implementation of the new floodplain. However, the new floodplain forcing substantially improved the ability of the model to reproduce the seasonality in flooded area (Fig. 3-2a-c); Nash Sutcliffe-Efficiency (NSE) and Root Mean Square Error (RMSE) were 0.91 and 12% respectively with the new floodplain forcing, compared to -0.75 and 32% with the old (Table 1).

Comparing model runs driven by the two different climate forcing, NCC and Princeton GPCC climate data, we find a similarly good performance as well. With both forcing data sets, we were able to recreate the observed mean magnitude and seasonality in discharge at Obidos (1980-2000) (Fig. 3-1 a, b) and flooded area in the central (Fig. S1) Amazon (1981-1996) (Fig. 3-2 a, b).

While the model was mostly able to reproduce the observed interannual variation in discharge, there was some minor difference in performance related to the choice of climate forcing (Figure 4, Table S1). The simulation driven by the Princeton GPPC data had an NSE of 0.79 and a RMSE of 4% against observations, compared to 0.50 and 7% for the NCC run (Figure 4, Table S1). The year with the highest observed discharge was 1989 with a mean of 199 10^3 m^3s^{-1}. The Princeton GPCC run correctly simulated 1989 as the year with the highest discharge, with a mean of 194 10^3 m^3s^{-1}. The NCC run ranks 1989 as the year with the second highest discharge, and actually predicts a higher 1989 mean discharge of 203 10^3 m^3s^{-1}. With NCC, the year with highest discharge is 1982, which is the 5th highest discharge in the observed time series. Conversely, the NCC simulation correctly modelled 1992 as the year with the lowest discharge (146 10^3 m^3s^{-1}) while the run driven with Princeton ranked 1992 second lowest (Figure 4, Table S1). It is important to note that the differences in observed discharge between both the highest (1989) and second highest (1994), and lowest (1992) and second lowest (1983) are minor (Figure 4, Table S1).

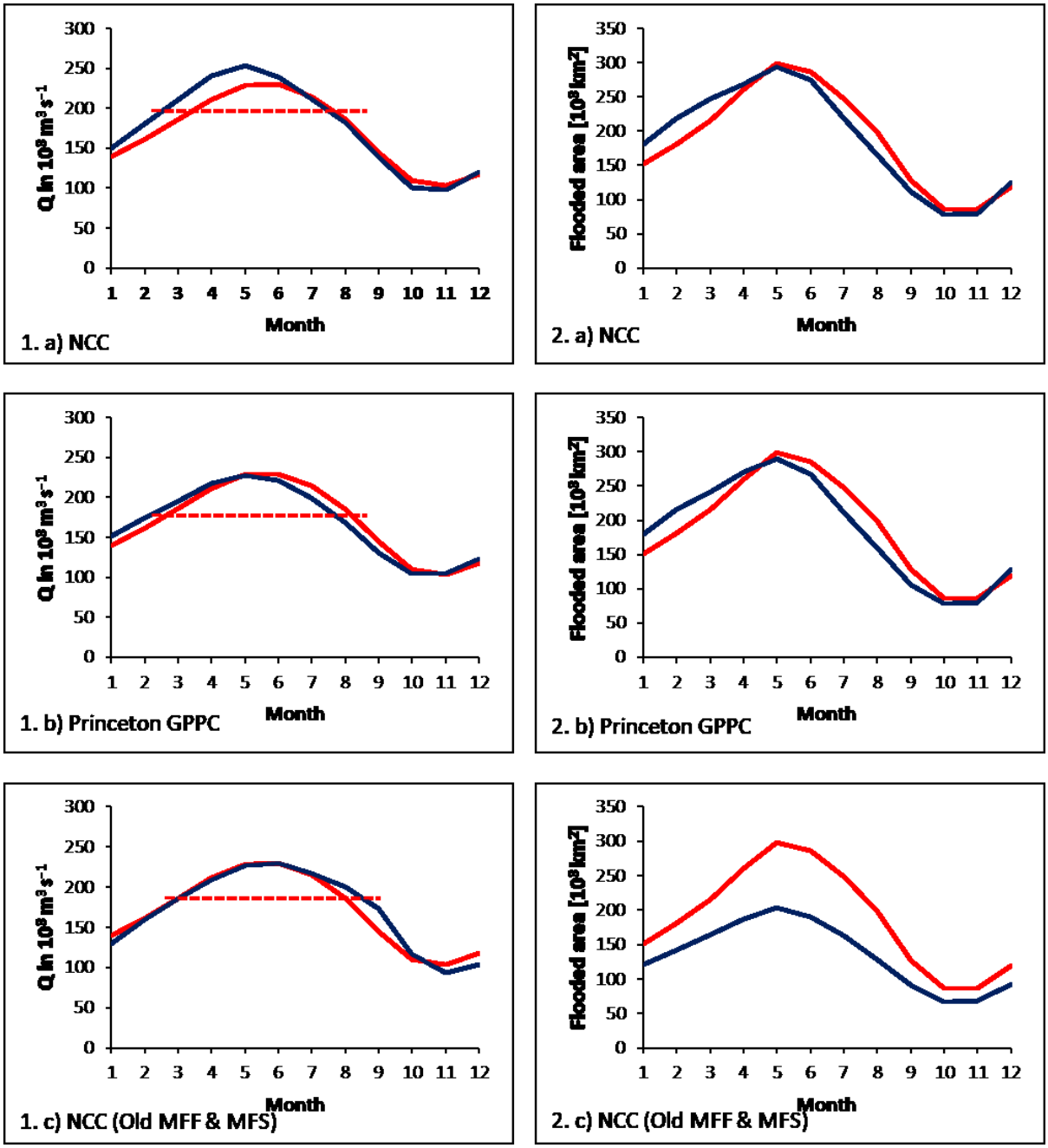

Figure 3- 1: Seasonality of simulated *versus* observed discharge (Cochonneau et al., 2006) at Obidos (1980-2000 monthly mean), with a) NCC climate forcing with standard MFF b) Princeton GPCC climate forcing with standard MFF and c) NCC with old MFF & MFS. 2: Seasonality of simulated versus observed flooded area (Melack et al., 2011) in the central Amazon basin (1981-1996 monthly mean) with a) NCC climate forcing with standard MFF b) Princeton GPCC climate forcing with standard MFF and c) NCC with old MFF & MFS.

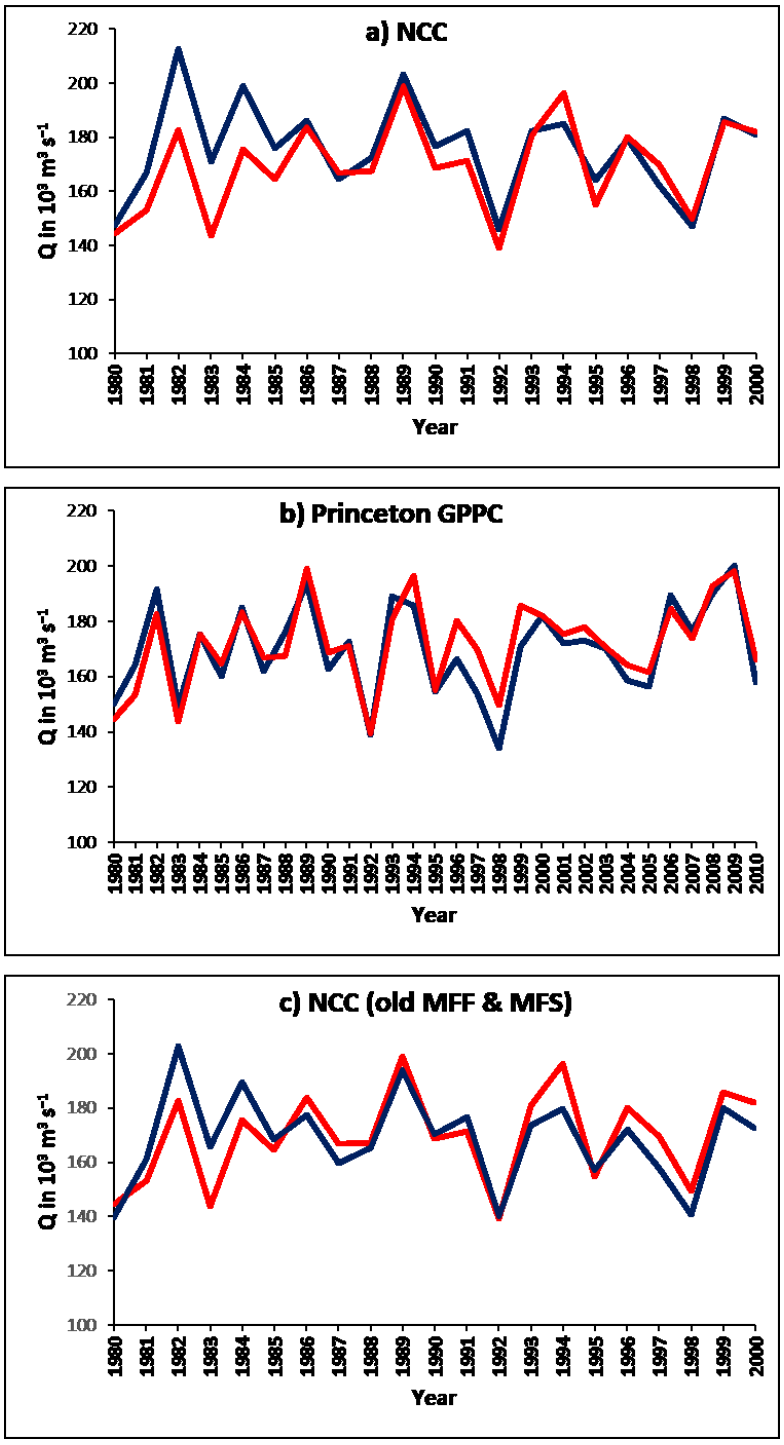

Figure 4. Annual variation of simulated vs observed discharge (Cochonneau et al., 2006) at Obidos (1980-2000) for a); run with NCC climate forcing with standard MFF, b) Princeton GPCC climate forcing with standard MFF and c) NCC climate forcing with old MFF & MFS

Table 1. Performance statistics for modelled versus observed discharge Q at Obidos and flooded area in the central Amazon basin for different climate forcing configurations

	Seasonality in Q at Obidos (1980-2000)			Flooded area in central Amazon (1981-1996)			Interannual variation in Q at Obidos (1980-2000)		
Climate forcing	RSME	NSE	R^2	RSME	NSE	R^2	RSME	NSE	R^2
NCC	9%	0.91	0.95	12%	0.91	0.91	7%	0.50	0.66
Princeton GPCC	6%	0.94	0.95	13%	0.89	0.90	4%	0.79	0.81
NCC (old MFF & MFS)	6%	0.95	0.95	32%	-0.75	0.97	6%	0.62	0.67

3.2 Carbon fluxes along the Amazon Basin

We estimate a long-term mean (1980-2000 across six model runs) NPP rate of 1,214 (1,204-1,223) g C m^{-2} yr^{-1} (range represents the variation caused by the combination of the two climate forcing and the three MFF forcing files; standard, MFF +7 and MFF-7), amounting to a total NPP of 6.81 (6.75-6.86) Pg C yr^{-1} for the entire Amazon Basin (5.6 x 10^6 km^2). If we only consider the uncertainty associated with climate forcing alone, the range is reduced to 6.77-6.85 Pg C yr^{-1}. The effect of the new MFF and MFS on NPP was negligible; mean annual NPP being 1,220 g C m^{-2} yr^{-1} (total of 6.84 Pg C yr^{-1}) and 1,222 g C m^{-2} yr^{-1} (total of 6.85 Pg C yr^{-1}) with the original (Lauerwald et al., 2017) and new forcing files, respectively, both driven by NCC. We estimate a mean annual soil heterotrophic respiration (SHR) of 5.87 (5.62-6.16) Pg C yr^{-1}. The new forcing file had a significantly greater effect on SHR than on NPP; the original forcing file (with NCC) produces a higher mean annual SHR of 6.30 Pg C

426 yr^{-1}, compared to 5.94 Pg C yr^{-1} (with NCC) this difference due to the greater suppression of
427 organic matter decomposition with the new MFF (Rueda-Delgado et al., 2006). We estimate
428 a mean annual throughfall DOC flux (TF) of 79 (78-79) Tg C yr^{-1}.

429 We simulate a mean annual (1980-2000) CO_2 evasion of 746 (526-998) Tg C yr^{-1} from the
430 water surfaces of the Amazon basin, a 97% increase from the 379 Tg C yr^{-1} produced with
431 the original ORCHILEAK configuration (Lauerwald et al., 2017). If we only include the
432 uncertainty associated with climate forcing, we produce a mean of 729 Tg C yr^{-1} and the
433 range is substantially reduced to 700-758 Tg C yr^{-1}, meaning that the majority of the
434 uncertainty in the evasion flux comes from the MFF forcing. We attribute approximately 75%
435 of the CO_2 evasion flux to the floodplain compared to 51% in the original study (Lauerwald
436 et al., 2017). With the new MFF forcing, we moderately improved the reproduction of
437 observed CO_2 evasion fluxes during low (monthly avg. discharge < yearly avg. discharge)
438 and high flow (monthly avg. discharge > yearly avg. discharge) periods at three sites in the
439 Amazon (Rasera et al., 2013, Fig. 5) (R^2 =0.80, RMSE = 1.4 µmol CO_2 m^{-2} s^{-1} vs R^2 =0.69,
440 RMSE = 1.9 µmol CO_2 m^{-2} s^{-}1, with new (a) and old MFF (c) respectively, both driven by
441 NCC). The performance was further improved with the Princeton GPCC climate data; R^2
442 =0.93, RMSE = 1.4 µmol CO_2 m^{-2} s^{-1} (Fig. 5, b).

443

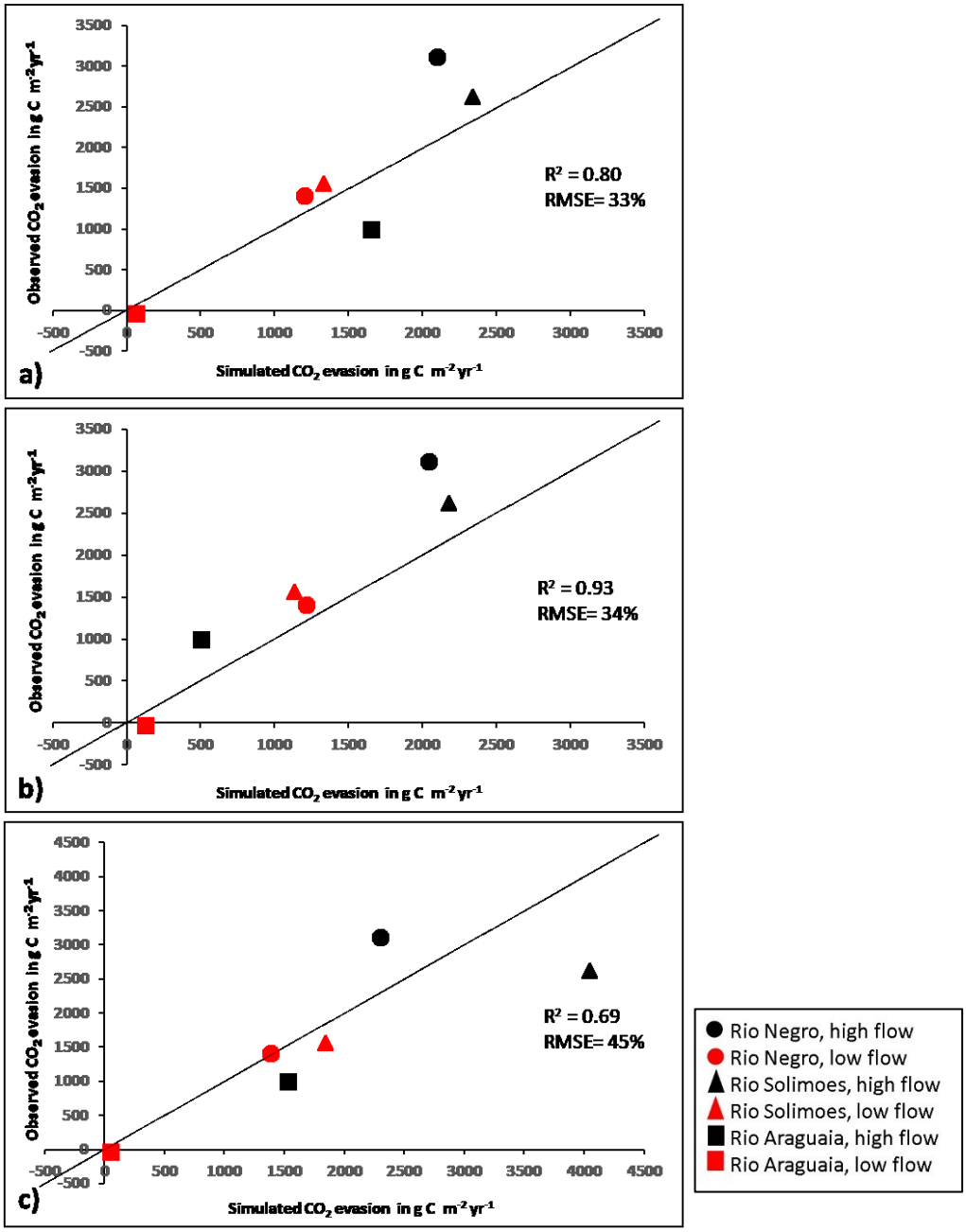

Figure 5. Observed versus simulated CO_2 evasion rates per water surface area for a); run with NCC climate forcing (standard MFF), b) Princeton GPCC climate forcing (standard MFF) and c) NCC climate forcing with old MFF & MFS. Observed data are from Rasera et al. (2013). Reported are means of the observed values, 2006 -2010. The simulated values refer to the mean evasion rate during low (monthly avg. discharge < yearly avg. discharge) and high flow periods (monthly avg. discharge > yearly avg. discharge) (1981–2000), see Figure 3. Note that the scale of the axes c) is slightly different to a) and b).

We simulate a mean annual (1980-2000) DOC export to the coast (downstream of Obidos) of 38 (33-44) Tg C yr^{-1}. In Figure 6, we compare simulated DOC flux against the observations at several sites (see Fig. S1 for locations) and find that the model can recreate the temporal

variation in DOC relatively well (Table S5). The effect of the new forcing files is mixed, with the performance improving at some sites but worsening at others (Fig. 6). The largest impact can be seen at Obidos where the new forcing files result in a substantially larger DOC flux during high flow. The model run using the old MFF and MFS appears to perform better at moderate discharge, while the new set up appears to perform better during periods when observed DOC is very high (i.e. 1990). Both appear to overestimate DOC flux at Obidos during low flow. We simulate a mean annual flux (to the coast) of dissolved CO_2 of 7.1 (6.8-7.7) Tg C yr^{-1}.

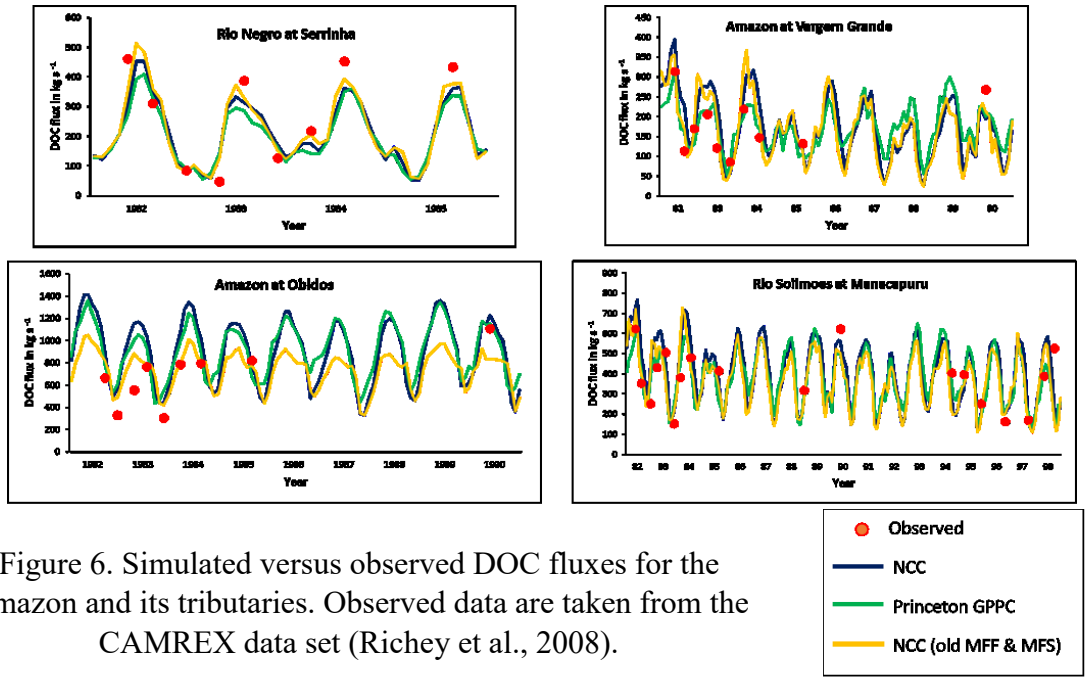

Figure 6. Simulated versus observed DOC fluxes for the Amazon and its tributaries. Observed data are taken from the CAMREX data set (Richey et al., 2008).

3.3 The net carbon balance of the Amazon Basin

The long-term mean (1980-2000) C balance; that is the components of the Net Ecosystem Production (NEP, equation 1), is presented in Fig. 7. We estimate a mean (1980-2000) NEP of 0.23 (0.15-0.33) Pg C yr^{-1} and a mean Net Biome Production (NBP, equation 2) of 0.04 (-

0.04-0.14) Pg C yr^{-1}. Using the original floodplain and swamp forcing files (with NCC), we estimate a mean annual NEP of 0.17 Pg C yr^{-1}. Using the same set up (with NCC) but with the new MFF and MFS forcing files we produce a higher sink of 0.21 Pg C yr^{-1}.

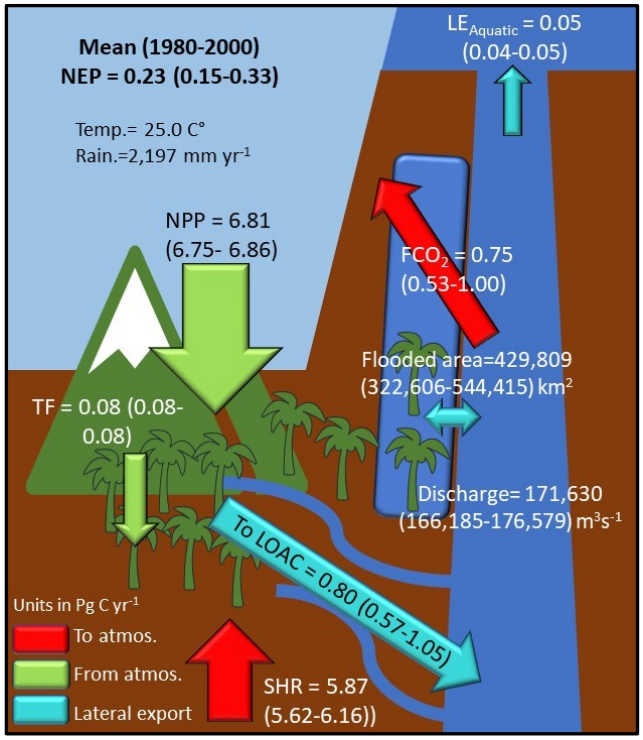

Figure 7. Simulated annual C budget (NEP) for the Amazon basin annual mean (1980-2000), where NEP is net ecosystem production, NPP is terrestrial net primary productivity, TF is throughfall, SHR is soil heterotrophic respiration, FCO_2 is aquatic CO_2 evasion, LOAC is C leakage to the land-ocean aquatic continuum (FCO_2 + to coast), and $LE_{Aquatic}$ is the export C flux to the coast. Numbers refer to mean across the six simulations while numbers in parentheses refer to range.

3.4 Interannual variation of the C fluxes within the Amazon Basin

Our results show considerable interannual variation in NPP, from a mean low of 6.41 (6.29-6.52) Pg C yr^{-1} in 1983, to a high of 7.16 (7.14- 7.16) Pg C yr^{-1} in 1996 (Fig.8-a), though the Princeton GPCC simulation, which runs until 2010, has several years (2006-2009 inclusive) with slightly higher NPP. This variation has a strong positive correlation with precipitation (detrended R^2 =0.48, $p<0.001$ with NCC; detrended R^2 =0.43, $p<0.0001$ with Princeton GPCC, Table S6 & S7, Fig. 9-a) and a strong negative correlation with temperature (detrended R^2 =0.56, $p<0.0001$ with NCC; detrended R^2 =0.43, $p<0.0001$ with Princeton GPCC, Table S6 & S7, Fig. 9-b). In addition, NPP is inversely correlated with the multivariate ENSO index (MEI, sum of monthly MEI from July of preceding year to June of concurrent year, detrended R^2 =0.40, $p<0.01$ with NCC; detrended R^2 =0.35, $p<0.001$ with

Princeton GPCC, Table S6 & S7, Fig. 9-c) (Wolter et al., 2011). We also find substantial interannual variation in SHR from a mean (across the two runs with new floodplain forcing) low of 5.69 (5.41- 6.03) Pg C yr^{-1} in 1982 to a high of 6.06 (5.91- 6.24) Pg C yr^{-1} in 1998 (Fig. 8-b). Conversely to NPP, SHR is positively correlated with temperature, and negatively correlated with rainfall, though these relationships are relatively weak (relationship with temperature not significant with NCC, detrended temperature R^2= 0.13 with Princeton GPCC, $p<0.05$; detrended rainfall R^2 =0.19, $p<0.05$ with NCC, detrended rainfall R^2 = 0.24, $p<0.01$ with Princeton GPCC).

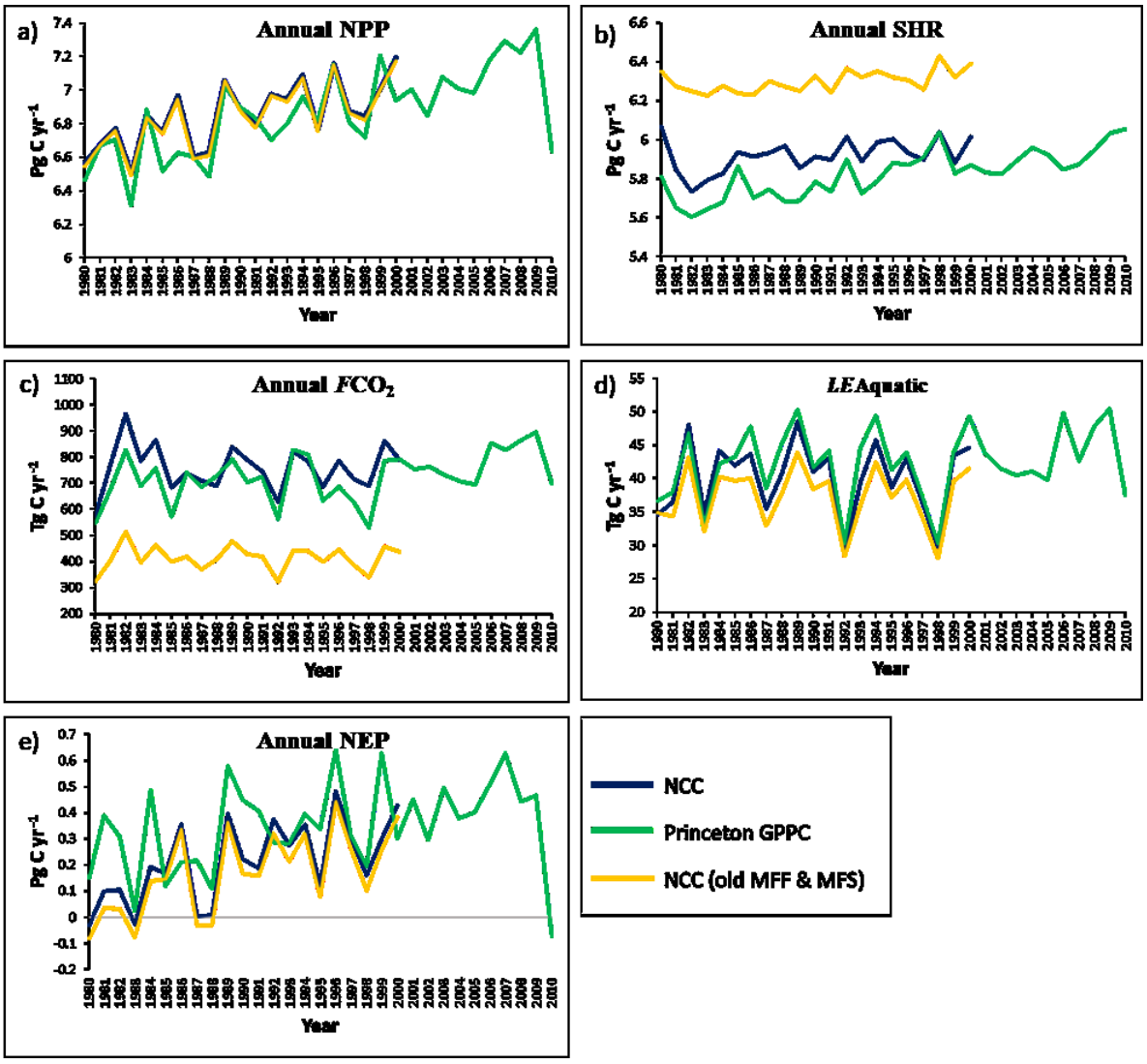

499 Figure 8. Simulated annual variation in NEP and its components over the Amazon Basin
500 from 1980-2000 (2010 in case of Princeton GPCC).

501

502 Our results also show considerable inter-annual (1980-2000) variation in inland water CO_2
503 evasion from a mean low of 571 (402- 759) Tg C yr^{-1} in 1980 to a high of 920 (633- 1,267)
504 Tg C yr^{-1} in 1982 (Fig.8-c), strongly correlated with precipitation (detrended $R^2 = 0.55$,
505 $p<0.001$ with NCC; detrended $R^2 = 0.64$, $p<0.0001$ with Princeton GPCC, Table S6 & S7)
506 and inversely correlated with temperature (detrended $R^2 = 0.21$, $p<0.05$ with NCC; detrended
507 $R^2 = 0.18$, $p<0.05$ with Princeton GPCC, Table S6 & S7). While both model runs rank 1982
508 as having the highest CO_2 evasion over the simulation period (1980-2000), there is some
509 divergence in regards to the lowest ranking year. The NCC run ranks 1980 lowest with 584
510 (422-759) Tg C yr^{-1} whereas the Princeton GPCC run ranks 1998 lowest with a total of 538
511 (399-685) Tg C yr^{-1}. In 1980 the Amazon rainy season was exceptionally dry (Andreoli et
512 al., 2012), while 1998 coincides with a strong El Nino event (Fig.9-c) and associated
513 anomalously low precipitation and high temperatures (Wenhong et al., 2011; Gloor et al.,
514 2013, 2015). Conversely, 1982 experienced an exceptionally wet rainy season (Andreoli et
515 al., 2012). These temporal patterns are also exhibited in the rainfall and temperature
516 parameters from both of the climate forcings used in this study (Fig.9).

517 At the interannual timescale, aquatic CO_2 evasion is only weakly to moderately correlated
518 with NPP (detrended $R^2 = 0.19$, $p<0.05$ NCC run; detrended $R^2 = 0.28$, $p<0.01$ with
519 Princeton GPCC run, Table S6 & S7) and therefore the proportion of NPP lost through the
520 LOAC is variable, ranging from 9% to 13%. In contrast, inland water CO_2 evasion is strongly
521 inversely correlated with SHR (detrended $R^2 = 0.76$, $p<0.0001$ NCC run; detrended $R^2 =$
522 0.66, $p<0.0001$ with Princeton GPCC run, Table S6 & S7), indicating that years with less
523 SHR have more evasion, and vice versa. Again, we find considerable interannual variation in

C flux to the coast (Fig. 8 d) displaying a similar pattern to aquatic CO_2 evasion (aquatic CO_2 evasion *versus* C flux to coast R^2 =0.48 for NCC, $p<0.001$; R^2 =0.64 $p<0.0001$ for Princeton GPCC, Table S6 & S7). Overall, and in relative terms, the LOAC fluxes show far greater interannual variation than the terrestrial C fluxes. For example, aquatic CO_2 evasion (NCC, 1980-2000) has a coefficient of variation (CV) of 11.7%, while the lateral flux of C to the coast has a CV of 13.6%. In contrast, NPP and SHR have a CV of only 2.9% and 1.5%, respectively.

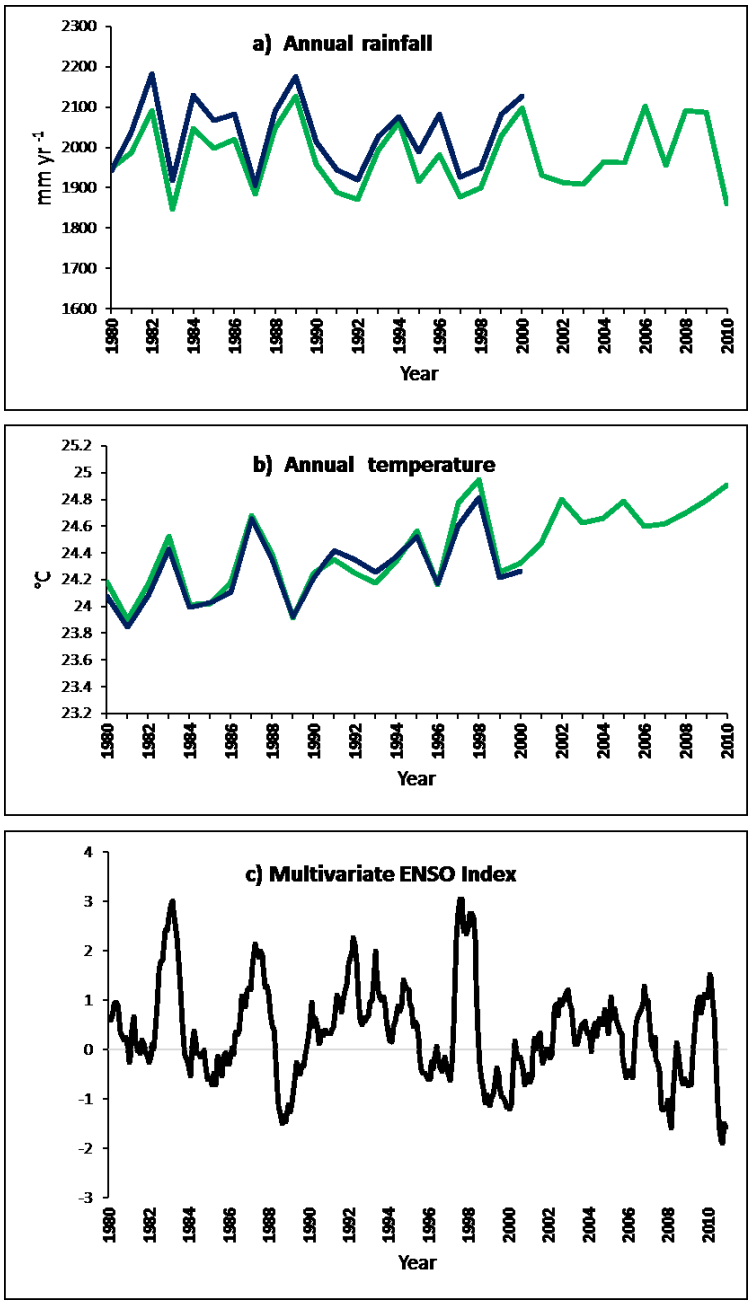

Figure 9. Interannual variation in a) rainfall and b) temperature. c) Monthly multivariate ENSO Index from 1980-2010 (Wolter et al., 2011)

As with its constituent components, simulated NEP shows considerable interannual variation (Figure 8-e) from a low of -0.05 (-0.11 – 0.03) Pg C yr^{-1} in 1983 to a high of 0.52 (0.41- 0.64) Pg C yr^{-1} in 1996. NEP is positively correlated with rainfall (detrended $R^2 = 0.27$, $p<0.05$ NCC run; detrended $R^2 = 0.25$, $p<0.01$ with Princeton GPCC run, Table S6 & S7) and negatively correlated with temperature (detrended $R^2 = 0.45$, $p<0.001$ NCC run; detrended $R^2 = 0.41$, $p<0.001$ with Princeton GPCC run, Table S6 & S7). The association with ENSO (detrended $R^2 = 0.35$, $p<0.01$ NCC run; detrended $R^2 = 0.26$, $p<0.01$ with Princeton GPCC run, Table S6 & S7) can be clearly seen in the simulated time series of NEP. Of the top six years with the lowest NEP (largest source of C to the atmosphere), four coincide with strong El Nino events, namely 1983, 1988, 1987 and 1998. Conversely, several of the years with the highest NEP (largest sink of atmospheric CO_2) take place during La Nina events, notably the strong La Nina event of 1988-1989, which results in the second highest simulated NEP; note that 2011 was one of the strongest La Nina on record but is not included in our forcing period. Taking the Princeton GPCC run alone, 2010 has the lowest NEP being a net CO_2 source to the atmosphere of -0.12 Pg C yr^{-1} (-0.14- -0.07) and coincides with another El Nino event combined with anomalously high Atlantic sea surface temperatures (SSTs) (Lewis et al., 2011).

We diagnosed the covariance between aquatic CO_2 evasion and the terrestrial C balance (defined as NPP-SHR) to determine how the variance in aquatic CO_2 evasion contributes to the overall variance in NEP across the simulation period. We find a negative covariance between aquatic CO_2 evasion and the terrestrial C balance of -0.024 and -0.022 for NCC and Princeton GPCC, respectively. Moreover, the terrestrial C balance is substantially more

557 sensitive to changes in both precipitation and temperature than NEP (Tables S8-S11). For
558 example (NCC run, Table S8), across the Amazon basin we find that the terrestrial C balance
559 increases by 120 Tg C yr^{-1} for every 100mm increase in rainfall, while NEP only increases by
560 57 Tg C yr^{-1}. Note that these values are based on simple linear regression and thus the
561 sensitivity to rainfall may be exaggerated but this is the case for both values.

562 As a consequence of this change in sensitivity, the variation of the budget is less pronounced
563 once the aquatic components are incorporated; the terrestrial C balance has a SD of 0.20 Pg C
564 yr^{-1} and 0.24 Pg C yr^{-1} with NCC and Princeton GPCC respectively, while NEP has a SD of
565 0.15 Pg C yr^{-1} and 0.17 Pg C yr^{-1}. These results concur with the idea of CO_2 evasion having a
566 moderating effect on overall heterotrophic respiration and suggest that accounting for CO_2
567 evasion from the river-floodplain network dampens the interannual variation in NEP.

568

569 4. Discussion

570 Our value of mean (across two models) NPP rate of 1,214 g C m^{-2} yr^{-1} matches closely to
571 previous estimates in the Amazon. Rodig et al. (2018) estimated a mean annual NPP of 1,130
572 g C m^{-2} yr^{-1} using the forest gap FORMIND model, while a value of 1,030 g C m^{-2} yr^{-1} was
573 derived from MODIS remote-sensing data (Zhao & Running, 2010).

574 Our estimate of mean total annual aquatic CO_2 evasion of 746 (526-998) Tg C yr^{-1} is
575 relatively close to the 800 Tg C yr^{-1} proposed by Rasera et al. (2013) from upscaling of
576 observations, over a larger basin area of 6×10^6 km^2. If we adjust our estimate (calculated
577 across a smaller basin area of 5.6×10^6 km^2) to the same area, then we get a closer estimate
578 of 799 Tg C yr^{-1}. Moreover, if we only base our mean CO_2 evasion estimate on the same
579 years as Rasera et al. (i.e. 2006- 2010), we actually produce a larger value of 887 Tg C yr^{-1}
580 (based on Princeton GPCC run only). We also estimate a similar distribution of CO_2 evasion

between low and high flow periods (Table S4). Like those of Rasera et al. (2013), our results exhibit a strong seasonal cycle in CO_2 evasion, with the high flow season (monthly avg. discharge > yearly avg. discharge) contributing approximately 75% of the annual total. In contrast, our results are considerably higher than those of Richey et al. (Table S4). It is encouraging that our results are similar to those of Rasera et al. (2013) as their upscaling was based on an extensive 5-year field campaign where the flux of CO_2 was directly measured while those of Richey et al. (2002) were derived indirectly from pCO_2 measurements. In terms of flood extent, the Rasera et al. study used the same assumptions for water surface area as Richey et al (2002), who in turn used an older version (Hess et al., 2002) of the Hess et al. (2015) floodplain product use in this study.

For the central quadrant of the Amazon basin alone (area = 1.77×10^6 km^2), we simulate a mean annual aquatic CO_2 evasion (1980-2000) of 341 and 318 Tg C yr^{-1} with NCC and Princeton GPPC, respectively, close to the 360 Tg C yr^{-1} estimated by Rasera et al. (2013), but considerably higher than the 210 Tg C yr^{-1} of Richey et al. (2002) and the 229 Tg C yr^{-1} of Lauerwald et al. (2017). Our results concur with both previous upscaling studies that the central Amazon basin contributes approximately 45% of the basin wide aquatic CO_2 evasion (Table S4). The differences between our CO_2 evasion estimates and those of Richey et al. (2002) are largely due to gas exchange velocity; we applied a fixed k_{600} rate of 3.5 m day^{-1} for rivers, while they used very conservative gas exchange velocities of 1.2 to 2.3 m day^{-1}. Conversely, the differences between our results and those of Lauerwald et al. (2017) are largely a result of the increase in maximal fraction of floodplain (MFF) across the basin, and the resultant increase in direct C inputs to inundated areas from canopy through-fall, submerged litter and soils. Our estimated DOC export to the coast (downstream of Obidos) of 34 (34-44) Tg C yr^{-1} is relatively high; Lauerwald et al. (2017), Richey et al. (1990) and

Moreira-Turcq et al. (2003) estimated this flux at 23.4 Tg C yr^{-1} , 24.4 Tg C yr^{-1} and 27 Tg C yr^{-1}, respectively.

Our results for the mean NEP of 0.23 (0.15-0.33) generally concur with previous estimates. Tian et al. (1998) used the Terrestrial Ecosystem Model to estimate a mean annual NEP, without considering the LOAC loop of the carbon cycle (undisturbed ecosystems, 1980-1994), of 0.2 ±0.9 Pg C yr^{-1}. Another modelling study (S. Sitch, B. Smith and J. Kaplan, unpublished but cited in Prentice and Lloyd, 1998, page 620) also settled on a mean annual NEP of around 0.2 ±1.2 Pg C yr^{-1} over the same 15-year period. A 2016 review (Grace, 2016), compiled all of the existing literature to produce two estimates of the net C balance of the Amazon Basin; one 'bottom-up' approach using "plot data and remote sensing" and one 'top-down approach' using "aircraft-based measurements in the planetary boundary layer", the latter based on Gatti et al. (2014). These two approaches include perturbation fluxes such as deforestation and harvesting and evasion emissions in the atmospheric inversion estimate of Gatti et al. and are thus equivalent to our estimate of NBP. The bottom-up approach concludes that the Amazon Basin is a net C source to the atmosphere of 0.11 Pg C yr^{-1} when including land use change emissions but with an uncertainty of ± 0.16, in other words not markedly different from zero. The top-down approach came to a similar conclusion; that the Amazon is a net source to the atmosphere of only 0.06 Pg C yr^{-1} in a 'normal year' but only two years (2010 and 2011) were analyzed in Gatti et al. Again, the near neutral balance of Gatti et al. (2014) intrinsically includes aquatic CO_2 evasion (though not the lateral fluxes of C to the coast). They argue that the impact of riverine CO_2 evasion on the Amazon C balance is minimal as the "riverine organic carbon loop is very nearly closed". In other words, the vast majority of LOAC export to aquatic systems return to the atmosphere before leaving the Amazon Basin. In summary, the results of Gatti et al. (2014) are arguably the most comparable to our own and it is therefore encouraging that we produce a relatively similar

NBP of 0.04 (-0.04-0.14) Pg C yr^{-1} (a difference of 100 Tg C^{-1} but with overlapping uncertainty ranges). It is important to note that ORCHILEAK does not incorporate methane fluxes. Indeed, if we include the recent estimate of the annual methane flux of approximately 40 Tg C^{-1} (Pangala et al., 2017) measured from the lower troposphere via aircraft; our NBP reduces to a neutral C balance.

While the new maximal fraction of floodplain (MFF) forcing leads to a dramatic increase in aquatic CO_2 evasion, it actually causes an overall decrease in the flux of CO_2 from the entire Amazon basin to the atmosphere. The greater inundation leads to a reduction in decomposition rates of litter, and soil organic matter. This suppression of organic matter decomposition has been observed in further field experiments (Dos Santos & Nelson, 2013), in addition to the study that informed the model configuration (Rueda-Delgado et al., 2006). This means that there is an additional net land C sink of approximately 40 Tg C yr^{-1} per year with the new floodplain compared to the old floodplain. While in a single year these differences are not so substantial, over long time periods they could lead to significant differences in the long-term net C balance of the Amazon.

We found that the interannual variation in NPP is positively correlated with rainfall and negatively correlated with temperature and our results concur with previous research showing that drought years have significantly lower NPP. In our outputs, two of the years with the lowest NPP are 1983 and 1988, coinciding with two strong El Nino events (1982-1983 and 1987-1988, Figure 9), and corroborating the findings of Asner & Townsend (2000) based on analysis of remote sensing data from 1982-1993. Previous modelling studies such as Botta et al (2002) have also found 1983 and 1988 to be years with anomalously low NPP in the Amazon. Moreover, a 2011 study that combined remote sensing and modelling (Potter et al., 2011) estimated that the 2010 drought caused a reduction in NPP in the Amazon of 7% relative to the La Nina year 2008, and we produce a similar value of 8% (0.58 Pg C).

655 However, a more recent study (Doughty et al., 2015) contradicts these findings. Doughty et
656 al. (2015) measured NPP, autotrophic respiration and heterotrophic respiration at thirteen 1ha
657 plots across South America from 2009-2011 and found that NPP remained relatively constant
658 throughout the period. They observed a reduction in CO_2 uptake via photosynthesis by 0.38
659 Pg C yr^{-1} during the 2010 drought, but this was offset by a concurrent reduction in
660 autotrophic respiration. They observed that the trees prioritised investment in growth (canopy
661 tissue), while they reduced autotrophic respiration investment in tissue maintenance and
662 defence, which ultimately may have caused an increase in tree mortality post drought
663 (Doughty et al., 2015). The inability of dynamic global vegetation models (DGVMs), as well
664 as remote sensing driven algorithms (Zhao & Running, 2010; Medlyn, 2011; Wang et al.,
665 2013) to represent these complex biological interactions is a major limitation in current
666 efforts to estimate NPP at the regional to global scale.

667 Our results show that both the seasonality and interannual variation in aquatic CO_2 evasion,
668 are closely correlated with discharge. In Figure 10 a) we show the relationship between
669 simulated monthly discharge and CO_2 evasion on the Madeira River at Porto Velho (R^2=0.81)
670 (see Fig. S1 for location). The Madeira basin contains approximately one fourth of
671 Amazonian wetlands (Melack and Hess 2010), including the extensive Llanos de Moxos and
672 was the subject of a recent CO_2 evasion field campaign (Almeida et al., 2017). Our
673 relationship follows a sigmoid curve where aquatic CO_2 evasion increases slowly at first
674 while discharge remains in bank. Once the river over-tops its banks, CO_2 evasion increases
675 rapidly before levelling out once the full area of the floodplain is saturated. Thus, at the basin
676 scale, aquatic CO_2 evasion not only increases because of larger floodplain surface area, but
677 also because of higher areal rates. This highlights the disproportionate importance of
678 floodplains as a source of C and supports the findings of Almeida et al. (2017, Fig. 10, b).
679 While they found a similarly strong relationship between observed discharge and aquatic CO_2

evasion at Porto Velho (R^2=0.85), as well as a similar range of values, the relationship does not follow precisely the same shape as ours. Their increase in evasion rate is more gradual and they do not observe a plateauing of CO_2 evasion above a certain discharge. This perhaps suggests that we underestimate the maximum extent of the floodplain in this specific model grid, and indeed, the location of Porto Velho, is in the minority of model grids where the maximum inundation actually decreases with the implementation of the new MFF forcing file.

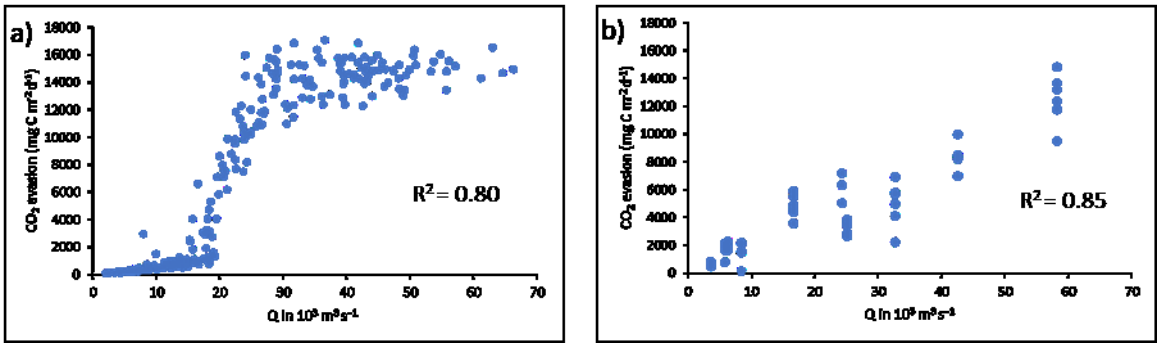

Figure 10. a); Monthly (1980-2000) simulated (NCC) aquatic CO_2 evasion vs simulated discharge on the Madeira River at Porto Velho and b); Observed aquatic CO_2 evasion vs observed on the Madeira River at Porto Velho, measured between 2009 and 2011.

The pattern of interannual variation in NEP over the 1980s and 1990s in our results is consistent with that found in previous modelling studies over the same period (Prentice and Lloyd, 1998; Tian et al., 1998). Interestingly we find smaller interannual variation than these previous modelling studies that did not include inland water fluxes, further supporting the idea that incorporating aquatic fluxes dampens the interannual variation in NEP. Indeed, a 2013 study (Wang et al., 2013) found results to suggest that some DGVMs overestimate the sensitivity of net ecosystem exchange (NEE) to precipitation. The relationship between our simulated NEP and precipitation is generally weaker than that found in previous models across the tropical region (Wang et al., 2013, in this case NEE), and the addition of the

aquatic C fluxes appears to be at least partly responsible for this; the sum of terrestrial fluxes (NPP-SHR) is more strongly correlated with precipitation (detrended $R^2 = 0.58$, $p<0.0001$ NCC run; detrended $R^2 = 0.51$, $p<0.0001$ with Princeton GPCC run) than NEP (detrended $R^2 = 0.27$, $p<0.05$ NCC run; detrended $R^2 = 0.25$, $p<0.01$ with Princeton GPCC run), which includes aquatic components.

Despite some of the limitations of DGVMs discussed, namely their inability to fully capture the complex effects of droughts on NPP, the response of our model to drought events concurs with observational based studies, and most significantly to those based on the measurement of atmospheric CO_2 fluxes. The 2010 Amazon drought was one of the most severe ever recorded and related to another El Nino event, as well as anomalous SSTs (Lewis et al., 2011). Gatti et al. (2014) used small aircraft to measure CO_2 fluxes just above the Amazon rainforest (lower-troposphere) and found that in 2010, the Amazon basin was a net source to the atmosphere of 0.48± 0.18 Pg C yr^{-1}. A 2015 study (van der Laan-Luijkx et al., 2015), further constrained the results of Gatti et al. using remote sensing data and estimated a smaller atmospheric CO_2 source between 0.07 and 0.31 Pg C yr^{-1} for 2010. Based on our Princeton GPCC run, we similarly estimate that in 2010, the Amazon was an overall CO_2 source for the atmosphere of 0.33 (0.35 - 0.29) Pg C yr^{-1} (based on NBP). Additionally, using a combined remote sensing and modelling approach, Potter et al. (2011) estimated that the 2010 drought caused a loss of biomass in the Amazon of 0.5 Pg C yr^{-1} relative to the strong La Nina year of 2008, and we produce a similar NEP deficit 0.51 Pg C yr^{-1}.

In Figure 11, we show our simulated C budget for a drought year, 1998, and an anomalously wet year, 1989, to illustrate how both terrestrial and aquatic C fluxes react to climatic extremes. In 1989, high aquatic CO_2 evasion to the atmosphere driven by high rainfall and large floodplain inundation, partly offsets a relatively large terrestrial sink, caused by high terrestrial NPP and low SHR. In 1998 the opposite occurs; low rainfall results in a low flux of

CO_2 from inland waters to the atmosphere, which moderates a relatively high SHR flux and low terrestrial NPP. As previously noted, aquatic CO_2 evasion is highly sensitive to rainfall and in turn both discharge and inundation, and displays greater interannual variation than the terrestrial C fluxes. Aquatic CO_2 evasion is positively correlated with NPP but the two fluxes represent opposite signals in terms of C exchange with the atmosphere, while aquatic CO_2 evasion is inversely correlated to SHR, both fluxes being C sources for the atmosphere. For these two reasons, the aquatic fluxes generally act to compensate the difference between terrestrial NPP and SHR and thus dampen overall interannual variation in the net C balance.

Another process not accounted for in our model is C sequestration on floodplains. Interestingly, a 2003 study (Aalto et al., 2003) showed that, sediment accumulation on Amazon floodplains is closely linked to the ENSO cycle. Like our findings for aquatic CO_2 evasion, sediment accumulation was found to be higher during La Nina years, and most notably in 1988. Despite not accounting for this C sink term in our model, the comparison of our net C balance for the Amazon (NBP) against observations (Grace et al., 2016) suggests that if anything we are still underestimating the net flux of C from the Amazon basin to the atmosphere.

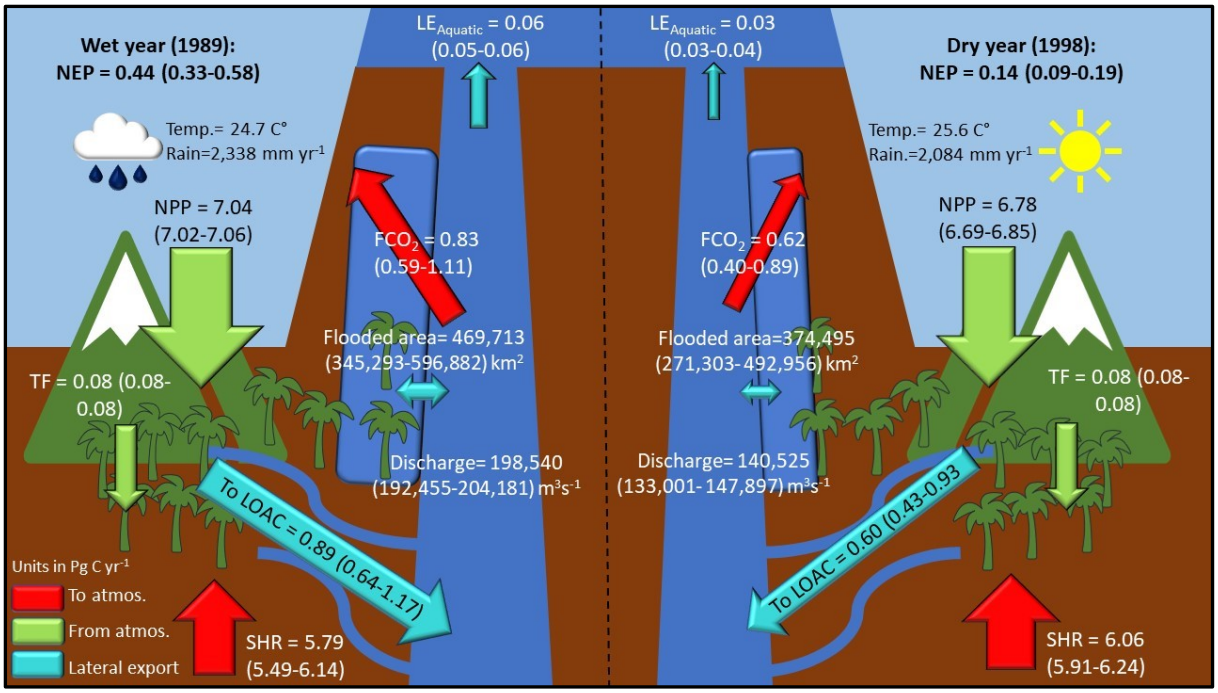

Figure 11. Simulated annual C budget for left; the Amazon basin for the year 1989, and right; the Amazon basin for the year 1998, where NEP is net ecosystem production, NPP is terrestrial net primary productivity, TF is throughfall, SHR is soil heterotrophic respiration, FCO_2 is aquatic CO_2 evasion, LOAC is C leakage to the land-ocean aquatic continuum (FCO_2 + to coast), and $LE_{Aquatic}$ is the export C flux to the coast. Numbers refer to mean across the six simulations while numbers in parentheses refer to range.

4.2 The importance of integrating the LOAC within the land carbon cycle

The Amazon is facing a number of threats including climate change, land use change and dam construction (Nobre et al., 2016). Climatic events such as droughts and floods are becoming more frequent (Marengo et al., 2011; Gloor et al., 2013; Zulkafli et al., 2016), while southern Amazonia has experienced a general lengthening of the dry season (Fu et al., 2013). The region is also undergoing a boom in dam construction with 140 dams under construction or already in operation, and a further 288 planned (Latrubesse et al., 2017) with direct impact on the C retention efficiency within the LOAC (Maavara et al., 2017). In addition, a recent study demonstrated that the lowland floodplain forests of the Amazon are less resilient to fires than terra firme forests (Flores et al., 2017).

For these reasons, it is vital that the flood dynamics of the Amazon can be correctly represented in biogeochemical models. The implementation of a new floodplain forcing file based on high resolution SAR data substantially improves our ability to accurately simulate the seasonality in observed flooding. Moreover, it leads to a 97% increase in our estimate of mean annual CO_2 evasion from the river-floodplain aquatic continuum and supports some larger previous estimates based on simple upscaling approaches (Table S4). Our results show that the LOAC fluxes, highly sensitive to hydrological variation, display greater interannual variation than the terrestrial C fluxes (NPP – SHR), and are thus disproportionately important to the overall variation of the net C balance, relative to their magnitude. We also find that the percentage of NPP lost to the LOAC is variable at the interannual timescale (Fig. 11).

Our results suggest that the linkage between the terrestrial and aquatic environment may be larger than previously thought and our estimate of aquatic CO_2 evasion from the Amazon is of a globally significant magnitude in terms of aquatic C fluxes. However, these results must be placed within the context of their overall impact on the net C balance of the Amazon Basin. While greater inundation increases aquatic CO_2 evasion, it simultaneously decreases the decomposition of organic matter in litter and soils and we show that the net impact of greater flooding is in fact a reduction in the flux of CO_2 from the Amazon basin to the atmosphere. It is during years with the lowest precipitation, often associated with El Nino events that highest net flux of CO_2 to the atmosphere are simulated. Indeed, we find that aquatic C fluxes partly compensate terrestrial C fluxes, and therefore moderate the overall interannual variation in NEP. Thus, DGVMs that do not account for aquatic fluxes may overestimate the magnitude of interannual variation in NEP. This calls for a fully integrated view of the land carbon cycle, which cannot be achieved with empirical studies alone and highlights the value of a model that can integrate the terrestrial and aquatic C cycles.

Acknowledgments

Financial support was received from the European Union's Horizon 2020 research and innovation program under the Marie Sklodowska- Curie grant agreement No. 643052 (C-CASCADES project). RL acknowledges funding from the European Union's Horizon 2020 research and innovation program under grant agreement no. 703813 for the Marie Sklodowska-Curie European Individual Fellowship "C-Leak." PR acknowledges funding from the Belgian Federal Science Policy Office (BELSPO), project "Global impacts of hydrological and climatic extremes on vegetation" (SAT-EX) – Belgian research programme for Earth Observation Stereo III.

References

Aalto, R., L. Maurice-Bourgoin, T. Dunne, D. R. Montgomery, C. A. Nittrouer, and J. L. Guyot (2003), Episodic sediment accumulation on Amazonian flood plains influenced by El Nino/Southern Oscillation, Nature, 425, 493–497, doi:10.1038/nature02002

Abril, G., Martinez, J.-M., Artigas, L. F., Moreira-Turcq, P., Benedetti, M. F., Vidal, L., … Roland, F. (2013). Amazon River carbon dioxide outgassing fuelled by wetlands. *Nature*, *505*, 395. Retrieved from http://dx.doi.org/10.1038/nature12797

Abril, G. and Borges, A. V.: Carbon leaks from flooded land: do we need to re-plumb the inland water active pipe?, Biogeosciences Discuss., https://doi.org/10.5194/bg-2018-239, in review, 2018.

Ahlström, A., Raupach, M. R., Schurgers, G., Smith, B., Arneth, A., Jung, M., ... Zeng, N. (2015). The dominant role of semi-arid ecosystems in the trend and variability of the land CO2 sink. Science, 348(6237), 895-899. DOI: 10.1126/science.aaa1668

Andreoli, R. V., Ferreira de Souza, R. A., Kayano, M. T. and Candido, L. A. (2012), Seasonal anomalous rainfall in the central and eastern Amazon and associated anomalous oceanic and atmospheric patterns. Int. J. Climatol., 32: 1193-1205. doi:10.1002/joc.2345

Almeida, R. M., Pacheco, F. S., Barros, N., Rosi, E., & Roland, F. (2017). Extreme floods increase CO2 outgassing from a large Amazonian river. *Limnology and Oceanography*, *62*(3), 989–999. https://doi.org/10.1002/lno.10480

Asner, G. P., Townsend, A. R., & Braswell, B. H. (2000). Satellite observation of El Niño effects on Amazon Forest phenology and productivity. *Geophysical Research Letters*, *27*(7), 981–984. https://doi.org/10.1029/1999GL011113

Aufdenkampe, A. K., Mayorga, E., Raymond, P. A., Melack, J. M., Doney, S. C., Alin, S. R., … Yoo, K. (2011). Riverine coupling of biogeochemical cycles between land, oceans, and atmosphere. *Frontiers in Ecology and the Environment*, *9*(1), 53–60. https://doi.org/10.1890/100014

Battin, T. J., Luyssaert, S., Kaplan, L. A., Aufdenkampe, A. K., Richter, A., & Tranvik, L. J. (2009). The boundless carbon cycle. *Nature Geoscience*, *2*, 598. Retrieved from https://doi.org/10.1038/ngeo618

Bond-Lamberty, B.P. and A.M. Thomson. 2014. A Global Database of Soil Respiration Data, Version 3.0. Data set. Available on-line [http://daac.ornl.gov] from Oak Ridge National Laboratory Distributed Active Archive Center, Oak Ridge, Tennessee, USA. http://dx.doi.org/10.3334/ORNLDAAC/1235

Botta, A., Ramankutty, N., & Foley, J. A. (2002). Long-term variations of climate and carbon fluxes over the Amazon basin. *Geophysical Research Letters*, *29*(9), 33–34. https://doi.org/10.1029/2001GL013607

Camino-Serrano, M., Guenet, B., Luyssaert, S., Janssens, I.A., 2018. ORCHIDEE-SOM: modeling soil organic carbon (SOC) and dissolved organic carbon (DOC) dynamics along vertical soil profiles in Europe. Geosci. Model Dev. 11, 937–957

Chou, C., Chiang, J. C. H., Lan, C.-W., Chung, C.-H., Liao, Y.-C., & Lee, C.-J. (2013). Increase in the range between wet and dry season precipitation. *Nature Geoscience*, *6*, 263. Retrieved from http://dx.doi.org/10.1038/ngeo1744

Ciais, P., Sabine, C., Bala, G., Bopp, L., Brovkin, V., Canadell, J., . . . (2013). Carbon and Other Biogeochemical Cycles. In T. F.. Stocker, D. Qin, G.-K. Plattner, M. Tignor, S. K. Allen, J. Boschung, A. Nauels, Y. Xia, V. Bex, and P. M. Midgley (Eds.), Climate change 2013: The physical science basis. Contribution of working group I to the fifth assessment report of the intergovernmental panel on climate change (pp. 465–570). Cambridge University Press, Cambridge.

Ciais, P., Gasser, T., Lauerwald, R., Peng, S., Raymond, P. A., Wang, Y., Zhu, D. (2017). Observed regional carbon budgets imply reduced soil heterotrophic respiration. Nature, in review.

Cochonneau, G., Sondag, F., Guyot, J.-L., Geraldo, B., Filizola, N., Fraizy, P., Laraque, A., Magat, P., Martinez, J.-M., Nor iega, L., Oliveira, E., Ordonez, J., Pombosa, R., Seyler, F., Sidgwick, J., and Vauchel, P.: The environmental observation and research project, ORE HYBAM, and the rivers of the Amazon basin, in: Climate Variability and Change – Hydrological Impacts, IAHS Publ. 308, edited by: Demuth, S., Gustard, A., Planos, E., Scatena, F., and Servat, E., IAHS Press, UK, 44–50, 2006

Cole, J. J., Prairie, Y. T., Caraco, N. F., McDowell, W. H., Tranvik, L. J., Striegl, R. G., & Melack, J. (2007). Plumbing the global carbon cycle: Integrating inland waters into the terrestrial carbon budget. Ecosystems,10(1), 172–185. https://doi.org/10.1007/s10021-006-9013-8

de Rosnay, P., Polcher, J., Bruen, M., and Laval, K.: Impact of a physically based soil water flow and soil-plant interaction representation for modeling large-scale land surface processes, J. Geophys. Res.-Atmos., 107, ACL3-1–ACL3-19, https://doi.org/10.1029/2001JD000634, 2002.

Doughty, C. E., Metcalfe, D. B., Girardin, C. A. J., Amézquita, F. F., Cabrera, D. G., Huasco, W. H., … Malhi, Y. (2015). Drought impact on forest carbon dynamics and fluxes in Amazonia. *Nature*, *519*, 78. Retrieved from https://doi.org/10.1038/nature14213

Dos Santos, A., & Nelson, B. (2013). Leaf decomposition and fine fuels in floodplain forests of the Rio Negro in the Brazilian Amazon. *Journal of Tropical Ecology, 29*(5), 455-458. doi:10.1017/S0266467413000485

d'Orgeval, T., Polcher, J., and de Rosnay, P.: Sensitivity of the West African hydrological cycle in ORCHIDEE to infiltration processes, Hydrol. Earth Syst. Sci., 12, 1387–1401, https://doi.org/10.5194/hess-12-1387-2008, 2008.

Drake, T. W., Raymond, P. A. and Spencer, R. G. (2018), Terrestrial carbon inputs to inland waters: A current synthesis of estimates and uncertainty. Limnol. Oceanogr., 3: 132-142. doi:10.1002/lol2.10055

Fasullo, J. T., Otto-Bliesner, B. L., & Stevenson, S. (2018). ENSO's Changing Influence on Temperature, Precipitation, and Wildfire In a Warming Climate. *Geophysical Research Letters*, *0*(ja). https://doi.org/10.1029/2018GL079022

Feldpausch. T., L., P. O., W., B. R. J., E., G., J., L., G., L., … A., V. V. (2016). Amazon forest response to repeated droughts. *Global Biogeochemical Cycles*, *30*(7), 964–982. https://doi.org/10.1002/2015GB005133

Foley, J. A., A. Botta, M. T. Coe, and M. H. Costa, El Niño–Southern oscillation and the climate, ecosystems and rivers of Amazonia, *Global Biogeochem. Cycles*, 16(4), 1132, doi: 10.1029/2002GB001872, 2002.

Fu, R., Yin, L., Li, W., Arias, P. A., Dickinson, R. E., Huang, L., … Myneni, R. B. (2013). Increased dry-season length over southern Amazonia in recent decades and its implication for future climate projection. *Proceedings of the National Academy of Sciences*, *110*(45), 18110–18115. https://doi.org/10.1073/pnas.1302584110

Gatti, L. V, Gloor, M., Miller, J. B., Doughty, C. E., Malhi, Y., Domingues, L. G., … Lloyd, J. (2014). Drought sensitivity of Amazonian carbon balance revealed by atmospheric measurements. *Nature*, *506*, 76. Retrieved from http://dx.doi.org/10.1038/nature12957

Gloor, M. *et al.* The carbon balance of South America: a review of the status, decadal trends and main determinants. *Biogeosciences* **9**, 5407–5430 (2012)

Gloor, M., R. J. W. Brienen, D. Galbraith, T. R. Feldpausch, J. Schöngart, J.-L. Guyot, J. C. Espinoza, J. Lloyd, and O. L. Phillips (2013), Intensification of the Amazon hydrological cycle over the last two decades, *Geophys. Res. Lett.*, 40, 1729–1733, doi: 10.1002/grl.50377.

Gloor, M., J. Barichivich, G. Ziv, R. Brienen, J. Schöngart, P. Peylin, B. B. Ladvocat Cintra, T. Feldpausch, O. Phillips, and J. Baker (2015), Recent Amazon climate as background for possible ongoing and future changes of Amazon humid forests, *Global Biogeochem. Cycles*, 29, 1384–1399, doi:10.1002/2014GB005080.

Grace J. (2016) The Amazon Carbon Balance: An Evaluation of Methods and Results. In: Nagy L., Forsberg B., Artaxo P. (eds) Interactions Between Biosphere, Atmosphere and Human Land Use in the Amazon Basin. Ecological Studies (Analysis and Synthesis), vol 227. Springer, Berlin, Heidelberg

Guimberteau, M., Drapeau, G., Ronchail, J., Sultan, B., Polcher, J., Martinez, J.-M., … Vauchel, P. (2012). Discharge simulation in the sub-basins of the Amazon using ORCHIDEE forced by new datasets. *Hydrology and Earth System Sciences*, *16*(3), 911–935. https://doi.org/10.5194/hess-16-911-2012

Gumbricht, T., Roman-Cuesta, R. M., Verchot, L., Herold, M., Wittmann, F., Householder, E., Murdiyarso, D. (2017). An expert system model for mapping tropical wetlands and

peatlands reveals South America as the largest contributor. *Global Change Biology*, *23*(9), 3581–3599. https://doi.org/10.1111/gcb.13689

Hastie, A., Lauerwald, R., Weyhenmeyer, G., Sobek, S., Verpoorter, C., Regnier, P (2017). CO2 evasion from boreal lakes: Revised estimate, drivers of spatial variability, and future projections. *Global Change Biology*, *24*(2), 711–728. https://doi.org/10.1111/gcb.13902

Hess, L. L., Melack, J. M., Novo, E. M. L. M., Barbosa, C. C. F., and Gastil, M.: Dual-season mapping of wetland inundation and vegetation for the central Amazon basin, Remote Sens. Environ., 87, 404–428, 2003

HESS, L. L., MELACK, J. M., NOVO, E. M. L. M., BARBOSA, C. C. F., & GASTIL, M. (2015). LBA-ECO LC-07 JERS-1 SAR Flooded Wetlands and Vegetation, Amazon Basin: 1995-1996. ORNL Distributed Active Archive Center. https://doi.org/10.3334/ornldaac/1284

Kim, H. (2017). *Global Soil Wetness Project Phase 3 Atmospheric Boundary Conditions (Experiment 1)* [Data set]. Data Integration and Analysis System (DIAS). https://doi.org/10.20783/DIAS.501

Latrubesse, E. M., Arima, E. Y., Dunne, T., Park, E., Baker, V. R., d'Horta, F. M., … Stevaux, J. C. (2017). Damming the rivers of the Amazon basin. *Nature*, *546*, 363. Retrieved from http://dx.doi.org/10.1038/nature22333

Lauerwald, R., Laruelle, G. G., Hartmann, J., Ciais, P., & Regnier, P. A. G. (2015). Spatial patterns in CO2 evasion from the global river network. *Global Biogeochemical Cycles*, *29*(5), 534–554. https://doi.org/10.1002/2014GB004941

Lauerwald, R., Regnier, P., Camino-Serrano, M., Guenet, B., Guimberteau, M., Ducharne, A., … Ciais, P. (2017). ORCHILEAK (revision 3875): a new model branch to simulate carbon transfers along the terrestrial--aquatic continuum of the Amazon basin. *Geoscientific Model Development*, *10*(10), 3821–3859. https://doi.org/10.5194/gmd-10-3821-2017

Lehner, B. and Döll, P.: Development and validation of a global database of lakes, reservoirs and wetlands, J. Hydrol., 296, 1–22, https://doi.org/10.1016/j.jhydrol.2004.03.028, 2004.

Lewis, S. L., Brando, P. M., Phillips, O. L., van der Heijden, G. M. F. & Nepstad, D. he 2010 Amazon drought. Science 331, 554–554 (2011).

Li, W., Zhang, P., Ye, J., Li, L., & Baker, P. A. (2011). Impact of two different types of El Niño events on the Amazon climate and ecosystem productivity. *Journal of Plant Ecology*, *4*(1–2), 91–99. Retrieved from http://dx.doi.org/10.1093/jpe/rtq039

Marengo, J. A., J. Tomasella, L. M. Alves, W. R. Soares, and D. A. Rodriguez (2011), The drought of 2010 in the context of historical droughts in the Amazon region, *Geophys. Res. Lett.*, 38, L12703, doi:10.1029/2011GL047436.

966 Maavara, T., Lauerwald, R., Regnier, P., & Van Cappellen, P. (2017). Global perturbation of
967 organic carbon cycling by river damming, *8*, 15347. Retrieved from
968 http://dx.doi.org/10.1038/ncomms15347

969 Medlyn, B. E. (2011). Comment on {\textquotedblleft}Drought-Induced Reduction in Global
970 Terrestrial Net Primary Production from 2000 Through 2009{\textquotedblright}.
971 *Science*, *333*(6046), 1093. https://doi.org/10.1126/science.1199544

972 Melack, J.M., L.L. Hess, M. Gastil-Buhl, B.R. Forsberg, S.K. Hamilton, I.B.T. Lima, and
973 E.M.L.M. Novo. 2011. LBA-ECO LC-07 Monthly Mean Flooded Wetlands Habitat,
974 Central Amazon Basin: 1979-1996. ORNL DAAC, Oak Ridge, Tennessee, USA.
975 https://doi.org/10.3334/ORNLDAAC/1049

976 Moreira-Turcq, P., Seyler, P., Guyot, J. L., & Etcheber, H. (2003). Exportation of organic
977 carbon from the Amazon River and its main tributaries. *Hydrological Processes*, *17*(7),
978 1329–1344. https://doi.org/10.1002/hyp.1287

979 Nemani, R.R., et al., 2003: Climate-driven increases in global terrestrial net primary
980 production from 1982 to 1999. Science, 300, 1560–1563.

981 Ngo-Duc, T., Polcher, J., and Laval, K (2005).: A 53-year forcing data set for land surface
982 models, *J. Geophys. Res.-Atmos*., 110, D06116, https://doi.org/10.1029/2004JD005434

983 Nobre, C. A., Sampaio, G., Borma, L. S., Castilla-Rubio, J. C., Silva, J. S., & Cardoso, M.
984 (2016). Land-use and climate change risks in the Amazon and the need of a novel
985 sustainable development paradigm. *Proceedings of the National Academy of Sciences*,
986 *113*(39), 10759–10768. https://doi.org/10.1073/pnas.1605516113

987 Pangala, S. R., Enrich-Prast, A., Basso, L. S., Peixoto, R. B., Bastviken, D., Hornibrook, E.
988 R. C., … Gauci, V. (2017). Large emissions from floodplain trees close the Amazon
989 methane budget. *Nature*, *552*, 230. Retrieved from https://doi.org/10.1038/nature24639

990 Phillips, O. L., Aragão, L. E. O. C., Lewis, S. L., Fisher, J. B., Lloyd, J., López-González, G.,
991 … Torres-Lezama, A. (2009). Drought Sensitivity of the Amazon Rainforest. *Science*,
992 *323*(5919), 1344–1347. https://doi.org/10.1126/science.1164033

993 Potter, C., S. Klooster, C. Hiatt, V. Genovese, and J. C. Castilla-Rubio (2011), Changes in the
994 carbon clycle of the Amazon ecosystem during the 2010 drought, *Environ. Res. Lett.*, **6**,
995 doi:10.1088/1748-9326/6/3/034024.

996 Prentice, I., and J. Lloyd. 1998. C-quest in the Amazon Basin. Nature 396:619–620.

997 R Core Team. (2013). R: A language and environment for statistical computing. [Available at
998 http://www.r-project.org.]

999 Rasera, M. F. F. L., Krusche, A. V., Richey, J. E., Ballester, M. V. R., and Victória, R. L.
1000 (2013). Spatial and temporal variability of pCO2 and CO2 efflux in seven Amazonian
1001 Rivers. *Biogeochemistry*, *116*(1), 241–259. https://doi.org/10.1007/s10533-013-9854-0

Regnier, P., Friedlingstein, P., Ciais, P., Mackenzie, F. T., Gruber, N., Janssens, I. A., … Thullner, M. (2013). Anthropogenic perturbation of the carbon fluxes from land to ocean. *Nature Geosci*, *6*(8), 597–607. Retrieved from http://dx.doi.org/10.1038/ngeo1830

Resplandy, L., Keeling, R. F., Rödenbeck, C., Stephens, B. B., Khatiwala, S., Rodgers, K. B., … Tans, P. P. (2018). Revision of global carbon fluxes based on a reassessment of oceanic and riverine carbon transport. *Nature Geoscience*, *11*(7), 504–509. https://doi.org/10.1038/s41561-018-0151-3

Richey Jeffrey E. , Hedges John I. , Devol Allan H. , Quay Paul D. , Victoria Reynaldo , Martinelli Luiz , Forsberg Bruce R. , (1990), Biogeochemistry of carbon in the Amazon River, *Limnology and Oceanography*, 35, doi: 10.4319/lo.1990.35.2.0352.

Richey, J. E., Melack, J. M., Aufdenkampe, A. K., Ballester, V. M., & Hess, L. L. (2002). Outgassing from Amazonian rivers and wetlands as a large tropical source of atmospheric CO2. *Nature*, *416*, 617. Retrieved from http://dx.doi.org/10.1038/416617a

Richey, J.E., R.L. Victoria, J.I. Hedges, T. Dunne, L.A. Martinelli, L. Mertes, and J. Adams. 2008. Pre-LBA Carbon in the Amazon River Experiment (CAMREX) Data. ORNL DAAC, Oak Ridge, Tennessee, USA. https://doi.org/10.3334/ORNLDAAC/904

Rödig E, Cuntz M, Rammig A, Fischer R, Taubert F and Huth A. (2018). The importance of forest structure for carbon fluxes of the Amazon rainforest. *Environmental Research Letters*, *13*(5), 54013. Retrieved from http://stacks.iop.org/1748-9326/13/i=5/a=054013

Rueda-Delgado, G., Wantzen, K. M., and Tolosa, M. B.: Leaflitter decomposition in an Amazonian floodplain stream: Effects of seasonal hydrological changes, J. North Am. Benthol. Soc., 25, 233–249, https://doi.org/10.1899/0887 3593(2006)25[233:LDIAAF]2.0.CO;2, 2006.

Sanders, L. M., Taffs, K. H., Stokes, D. J., Sanders, C. J., Smoak, J. M., Enrich-Prast, A. , Macklin, P. A., Santos, I. R. and Marotta, H. (2017), Carbon accumulation in Amazonian floodplain lakes: A significant component of Amazon budgets?. Limnol. Oceanogr., 2: 29-35. doi:10.1002/lol2.10034

Sheffield, J., Goteti, G., & Wood, E. F. (2006). Development of a 50-Year High-Resolution Global Dataset of Meteorological Forcings for Land Surface Modeling. *Journal of Climate*, *19*(13), 3088–3111. https://doi.org/10.1175/JCLI3790.1

Tian, H., J. M. Melillo, D. W. Kicklighter, A. D. McGuire, J. V. K. Helfrich, B. Moore, and C. J. Vorosmarty. 1998. Effect of interannual climate variability on carbon storage in Amazonian ecosystems. Nature 396:664–667.

Tranvik, L. J., Downing, J. A., Cotner, J. B., Loiselle, S. A., Striegl, R. G., Ballatore, T. J., . . . Weyhenmeyer, G. A. (2009). Lakes and reservoirs as regulators of carbon cycling and climate. Limnology and Oceanography, 54(6 part 2), 2298–2314. https://doi.org/10.4319/lo.2009.54.6_part_2.2298

van der Laan-Luijkx, I. T., I. R. van der Velde, M. C. Krol, L. V. Gatti, L. G. Domingues, C. S. C. Correia, J. B. Miller, M. Gloor, T. T. van Leeuwen, J. W. Kaiser, et al. (2015), Response of the Amazon carbon balance to the 2010 drought derived with CarbonTracker South America, *Global Biogeochem. Cycles*, 29, 1092–1108, doi: 10.1002/2014GB005082.

Vörösmarty, C. J., Fekete, B. M., Meybeck, M., and Lammers, R. B.: Geomorphometric attributes of the global system of rivers at 30-minute spatial resolution, J. Hydrol., 237, 17–39, 2000.

Wang, W., Ciais, P., Nemani, R. R., Canadell, J. G., Piao, S., Sitch, S., White, M. A., Hashimoto, H., Milesi, C., and Myneni, R. B.: Variations in atmospheric CO2 growth rates coupled with tropical temperature, Proc. Natl. Acad. Sci. USA, 110, 13061–13066, doi:10.1073/pnas.1219683110, 2013.

Wolter, K., and M. S. Timlin, 2011: El Niño/Southern Oscillation behaviour since 1871 as diagnosed in an extended multivariate ENSO index (MEI.ext). *Intl. J. Climatology*, **31**, 14pp., 1074-1087

Zarfl, C., Lumsdon, A. E., Berlekamp, J., Tydecks, L., & Tockner, K. (2015). A global boom in hydropower dam construction. *Aquatic Sciences*, *77*(1), 161–170. https://doi.org/10.1007/s00027-014-0377-0

Zhao, M., & Running, S. W. (2010). Drought-Induced Reduction in Global Terrestrial Net Primary Production from 2000 Through 2009. *Science*, *329*(5994), 940–943. https://doi.org/10.1126/science.1192666

Zulkafli, Z., Buytaert, W., Manz, B., Rosas, C. V., Willems, P., Lavado-Casimiro, W., Guyot, J.-L., and Santini, W.: Projected increases in the annual flood pulse of the Western Amazon, Environ. Res. Lett., 11, 14013, doi:10.1088/1748-9326/11/1/014013, 2016.